JOURNAL OF COMPUTATIONAL PHYSICS 119, 75–93 (1995)

A Finite-Difference, Frequency-Domain Numerical Scheme for the Solution of the Gust Response Problem

JAMES R. SCOTT

NASA Lewis Research Center, Cleveland, Ohio 44135

AND

HAFIZ M. ATASSI

University of Notre Dame, Notre Dame, Indiana 46556

Received August 26, 1994

A numerical method is developed for solving subsonic flows with convected, three-dimensional vortical waves around lifting airfoils. The first-order method that is presented fully accounts for the distortion effects of the nonuniform mean flow on the convected vorticity. The unsteady velocity is split into a vortical component which is a known function of the upstream flow conditions and the Lagrangian coordinates of the mean flow, and an irrotational field whose potential satisfies a nonconstant-coefficient, inhomogeneous, convective wave equation. Using an elliptic coordinate transformation, the unsteady boundary value problem is solved in the frequency domain on grids which are determined as a function of the Mach number and reduced frequency. Extensive comparisons are made with known solutions to unsteady vortical flow problems, and it is seen that the agreement is in general very good for reduced frequencies ranging from zero to four.

1. INTRODUCTION

Most flows encountered in aerodynamics are high speed flows where the Reynolds number is large and the effects of viscosity are confined to small regions such as boundary layers and wakes. Because major portions of these flow fields are essentially inviscid and irrotational, potential flow theory has been used extensively by aerodynamicists in the analysis of flows about streamlined bodies. Today steady potential flow solvers are widely used in the design of aircraft wings, turbomachinery blades, and helicopter rotors.

In many real flow applications, however, the flow is not steady but unsteady. Frequently the unsteadiness in the flow is due to the occurrence of upstream vortical disturbances that are convected downstream and induce an unsteady flow field as they interact with the body. For an aircraft wing, such upstream flow distortion can be caused by atmospheric turbulence. For propeller and turbomachinery blades, the vortical disturbances may be caused by the viscous wakes of an upstream rotor or stator, installation effects, or upstream turbulence.

When viewed from the blade frame of reference, the upstream vortical disturbances will appear as propagating vorticity waves that are called gusts. There are a number of undesirable effects that can be associated with such vortical gusts. They will, for example, induce unsteady forces on the airfoil surface which can cause forced vibrations and radiate noise into the far field. In some instances, the impinging gusts may cause flow separation and loss of aerodynamic performance. For rotating blades, the fundamental frequency of the upstream disturbances will equal the blade passing frequency. If the frequency of the aerodynamic excitation equals a natural frequency of the rotating blades and the amplitude is sufficient, then catastrophic structural failure may results.

Another possible source of unsteadiness in the flow is the unsteady motion of the airfoils or blades themselves. Such unsteady structural motion can be caused by structure-borne vibrations as well as the flow-induced oscillations described above. There can also be unsteady interactions between the airfoil motion and the incident disturbances which can dampen or increase the magnitude of the airfoil unsteady motion.

Because of the undesirable effects associated with these unsteady flows, there is considerable interest in controlling and understanding the aerodynamic excitations which can cause such unsteady blade motion.

Up until recently, most numerical efforts to solve these kinds of unsteady flows concentrated on potential methods. The early work dealt with solving the unsteady small disturbance potential equation as a way of obtaining the unsteady flow around oscillating airfoils or cascades. Later work was directed toward solving the linearized unsteady potential equation and the unsteady full potential equation. Potential methods have proven to work well for flutter-induced oscillating airfoil problems, but unfortunately they cannot be used to describe vortical flows. Previous potential formulations which have been modified to include the effects of the upstream vorticity have invoked the

0021-9991/95 $6.00

linear thin airfoil approximation and assumed that the imposed vortical gust is convected without distortion by the nonuniform mean flow. This was the approach first used by Horlock [1] and later by McCroskey and Goorjian [2] and McCroskey [3]. However, as shown by Goldstein and Atassi [4], Atassi [5], and Scott and Atassi [6], the assumption that the gust is convected without distortion is not justified and is a poor approximation for flows with a spatially varying mean flow. This is especially true for turbomachinery and propeller flow fields where the blades are heavily loaded and there are strong mean flow gradients.

In the past few years, computational efforts in unsteady aerodynamics have concentrated on the so-called primitive variable methods in which the unsteady Euler or Navier–Stokes equations are solved in time along with certain specified boundary conditions. Primitive variable methods, of course, offer the advantage of being equally well suited to both irrotational and vortical flows. The main difficulty associated with these methods, however, is that they are too expensive to be used for routine engineering calculations such as are encountered in design work. For some engineering applications, it may even be impossible to solve the full Euler or Navier–Stokes equations due to limitations in available computational resources. Another concern is the loss of accuracy due to uncertainties about physically correct far-field boundary conditions.

Recently, Scott and Atassi [6] and Scott [7] have presented a linearized unsteady aerodynamic analysis, based on Atassi and Grzedzinski's [8] modification of Goldstein's [9] velocity splitting, for the solution of unsteady aerodynamic flow fields. Our approach offers the computational efficiency of potential methods, but at the same time accounts for the convection and distortion of the upstream vorticity by the nonuniform mean flow. Our formulation also offers the advantage of being suitable for both irrotational and vortical flows. In addition, since we linearize about the nonuniform mean flow, the full nonlinear effects of the steady flow are accounted for. Because of these features, the linearized analysis that we have developed is an ideal choice for the numerical solution of unsteady aerodynamic flow problems.

In [6, 7] we presented in detail the mathematical formulation on which the present approach is based. We also presented numerical solutions to the gust response problem for a large variety of flow configurations. Our numerical results showed in detail the effects of airfoil thickness, angle of attack, camber, and Mach number on the unsteady lift and moment of isolated airfoils subjected to a periodic vortical gust.

In this paper we summarize the mathematical formulation and present the details of the frequency domain numerical scheme that has been developed by the authors to implement the linearized analysis presented in Refs. [6, 7]. We summarize the linearized boundary value problem in the following section. Following that, we present the frequency domain numerical scheme and conclude with a discussion of numerical results.

2. LINEARIZED UNSTEADY AERODYNAMIC FORMULATION

Consider an inviscid, compressible flow past a two-dimensional airfoil placed at nonzero incidence to a stream with uniform upstream velocity U_∞ in the x_1 direction. We assume in the present discussion that the fluid is an ideal, nonheat-conducting gas with constant specific heats and that any shock waves that appear are sufficiently weak that entropy changes can be neglected. Under the above assumptions there will be a steady potential flow around the airfoil so that we may write

$$\mathbf{U}_0(\mathbf{x}) = \nabla\Phi_0, \tag{2.1}$$

where 0 subscripts are used to denote steady mean flow quantities.

Let us assume that far upstream an unsteady convected vortical disturbance is imposed on the flow. The only restriction that we place on the upstream disturbance is that it can be expressed as a generalized Fourier integral so that we may write

$$\mathbf{u}_\infty(\mathbf{x} - \mathbf{i}U_\infty t) = \int_{\mathbf{k}} \mathbf{a}(\mathbf{k}) e^{i\mathbf{k}\cdot(\mathbf{x}-\mathbf{i}U_\infty t)} d\mathbf{k}, \tag{2.2}$$

and, in addition, that its characteristic length scale l' and velocity u_∞ are such that the condition

$$\frac{c}{U_\infty} \ll \frac{l'}{u_\infty} \tag{2.3}$$

is satisfied, where c is the airfoil chord length. We thus require that the time scale associated with the mean flow be an order of magnitude less than the time scale associated with the upstream unsteady disturbances. Since our concern is with flows that have large scale upstream disturbances in which l' is the same order of magnitude as the chord length c, condition (2.3) essentially reduces to the requirement that $u_\infty \ll U_\infty$.

Since we present a linearized mathematical formulation, we may without loss of generality consider a single Fourier component of the incident vortical disturbance and solve for more general disturbances by superposition. We therefore consider incident vortical gusts of the form

$$\mathbf{u}_\infty = \mathbf{a} e^{i\mathbf{k}\cdot(\mathbf{x}-\mathbf{i}U_\infty t)}, \tag{2.4}$$

where $\mathbf{a}$ and $\mathbf{k}$ must satisfy

$$\mathbf{a}\cdot\mathbf{k} = 0 \tag{2.5}$$

to ensure that the continuity equation is satisfied [10]. For a two-dimensional lifting airfoil, the expression of the gust may not reduce to Eq. (2.4) [4]. However, since a two-dimensional airfoil is an approximation of a large-aspect-ratio real airfoil,

(2.4) will be valid at a distance that is large compared to the airfoil span [5].

For general flow fields in which $\mathbf{U}_0$ varies spatially as a function of $\mathbf{x}$, it is convenient to formulate the unsteady boundary value problem in terms of the Lagrangian coordinates of the mean flow. For the case of two-dimensional mean flow, we introduce the new independent variables $(X_1, X_2, X_3) = \mathbf{X}$, where

$$X_2 = \frac{\Psi_0}{\rho_\infty U_\infty} \tag{2.6}$$

and

$$X_3 = x_3, \tag{2.7}$$

where Ψ_0 is the stream function of the mean flow and x_3 is the spatial coordinate in the spanwise direction. The component X_1 is defined by

$$X_1 = U_\infty \Delta, \tag{2.8}$$

where Δ is the Darwin–Lighthill "drift" function [11, 12], which can be expressed in terms of Φ_0 and Ψ_0 as

$$\Delta = \frac{\Phi_0}{U_\infty^2} + \int_{-\infty}^{\Phi_0} \left(\frac{1}{U_0^2} - \frac{1}{U_\infty^2} \right) d\Phi_0, \tag{2.9}$$

where the integration is carried out on $\Psi_0 = \text{const}$. The difference in the value of Δ between two points on a streamline is the time it takes a mean flow fluid particle to traverse the distance between those two points. Note that for the thin airfoil case in which the mean flow is a uniform parallel flow, the components of $\mathbf{X}$ reduce precisely to the spatial coordinates.

We assume that the total unsteady flow field can be represented by

$$\mathbf{U}(\mathbf{x}, t) = \mathbf{U}_0(\mathbf{x}) + \mathbf{u}(\mathbf{x}, t) \tag{2.10}$$

$$p(\mathbf{x}, t) = p_0(\mathbf{x}) + p'(\mathbf{x}, t) \tag{2.11}$$

$$\rho(\mathbf{x}, t) = \rho_0(\mathbf{x}) + \rho'(\mathbf{x}, t) \tag{2.12}$$

$$s(\mathbf{x}, t) = s_0 + s'(\mathbf{x}, t), \tag{2.13}$$

where the entropy s_0 is constant, and $\mathbf{u}$, p', ρ', and s' are the unsteady perturbation velocity, pressure, density and entropy, respectively. Quantities with 0 subscripts are the steady mean flow quantities which are assumed to be known. Note that these quantities obey the steady nonlinear equations of motion, so that the linearization of the unsteady flow is about the fully nonlinear mean flow.

Substituting (2.10)–(2.13) into the nonlinear Euler equations and neglecting products of small quantities, one obtains the linearized continuity, momentum, and entropy conservation equations

$$\frac{D_0 \rho'}{Dt} + \rho' \nabla \cdot \mathbf{U}_0 + \nabla \cdot (\rho_0 \mathbf{u}) = 0 \tag{2.14}$$

$$\rho_0 \left(\frac{D_0 \mathbf{u}}{Dt} + \mathbf{u} \cdot \nabla \mathbf{U}_0 \right) + \rho' \mathbf{U}_0 \cdot \nabla \mathbf{U}_0 = -\nabla p' \tag{2.15}$$

$$\frac{D_0 s'}{Dt} = 0, \tag{2.16}$$

where $D_0/Dt = \partial/\partial t + \mathbf{U}_0 \cdot \nabla$ is the convective derivative associated with the mean flow.

It is shown in Refs. [8, 9] that if the unsteady velocity is decomposed into the sum of a known vortical component and an unknown potential component, then the problem for determining the unsteady flow may be reduced to solving a single, nonconstant coefficient, inhomogeneous convective wave equation which may be written

$$\frac{D_0}{Dt} \left(\frac{1}{c_0^2} \frac{D_0 \phi}{Dt} \right) - \frac{1}{\rho_0} \nabla \cdot (\rho_0 \nabla \phi) = \frac{1}{\rho_0} \nabla \cdot (\rho_0 \mathbf{u}^{(R)}), \tag{2.17}$$

where

$$\mathbf{u}(\mathbf{x}, t) = \mathbf{u}^{(R)} + \nabla \phi. \tag{2.18}$$

The unsteady pressure is related to ϕ through the equation

$$p' = -\rho_0(\mathbf{x}) \frac{D_0 \phi}{Dt}. \tag{2.19}$$

The vortical velocity $\mathbf{u}^{(R)}$ is a known function of the mean flow Lagrangian coordinates and the upstream vortical disturbances and is given by [8]

$$\mathbf{u}^{(R)} = [\nabla(\mathbf{a} \cdot \mathbf{X})] e^{i\mathbf{k} \cdot (\mathbf{X} - i U_\infty t)} + \nabla \tilde{\phi}, \tag{2.20}$$

where

$$\tilde{\phi} = \frac{i}{k_1} \left(a_1 + \frac{a_2 k_1 - a_1 k_2}{1 + i a_0 U_\infty k_1} \frac{1 - e^{-ik_2 X_2}}{k_2} \right) e^{i\mathbf{k} \cdot (\mathbf{X} - i U_\infty t)} \tag{2.21}$$

and

$$\mathbf{a} = (a_1, a_2, a_3), \quad a_0 = -(\partial U_0 / \partial n)_s^{-1}. \tag{2.22}$$

Here n denotes the direction of the outward unit normal, S denotes the stagnation point near the airfoil leading edge, and $U_0 = |\mathbf{U}_0|$ is the magnitude of the mean velocity. ($\nabla \phi$ is included to eliminate the singularity that occurs in the boundary condition of Goldstein's original formulation. See [8] for details.)

Finally, the potential ϕ must satisfy the boundary conditions

$$\nabla\phi \cdot \mathbf{n} = 0 \quad \text{airfoil surface} \tag{2.23}$$

$$\frac{D_0}{Dt}(\Delta\phi) = 0 \quad \text{wake} \tag{2.24a}$$

$$\Delta[\nabla\phi \cdot \mathbf{n}] = 0 \quad \text{wake} \tag{2.24b}$$

$$\nabla\phi \to -\nabla\tilde{\phi} \quad \text{as } x_1 \to -\infty, \tag{2.25}$$

where Eq. (2.23) is the impermeability condition at the airfoil surface, Eqs. (2.24a) and (2.24b) impose continuity of the pressure and normal velocity, respectively, across the wake, and Eq. (2.25) ensures that $\mathbf{u}(\mathbf{x}, t) \to \mathbf{u}_\infty(\mathbf{x}, t)$ as $x_1 \to -\infty$.

The linearized boundary value problem for the unsteady gust response problem thus consists of the governing equation (2.17) and boundary conditions (2.23)–(2.25), together with the requirement that ϕ be continuous at the airfoil trailing edge.

3. NUMERICAL SCHEME

3.1. *Formulation and Nondimensionalization of the Boundary Value Problem*

For numerical purposes it is necessary to reformulate the boundary value problem presented in the previous section into a form more suitable for numerical computations. Of particular concern is condition (2.25). In order to facilitate the implementation of the far-field boundary condition, it is convenient to replace ϕ by a function whose gradient vanishes as $r \to \infty$, where r is the distance from the airfoil center.

To this end, we introduce the potential functions ϕ_1 and ϕ_2, where

$$\phi = \phi_1 - \phi_2 \tag{3.1}$$

and ϕ_2 is a known function which is constructed such that

$$|\phi_2 - \tilde{\phi}| \to 0 \quad \text{as } r \to \infty. \tag{3.2}$$

Equation (3.1), together with conditions (2.25) and (3.2), then shows that the new potential function ϕ_1 will satisfy

$$\nabla\phi_1 \to \nabla\phi_2 - \nabla\tilde{\phi} \to 0 \quad \text{as } r \to \infty. \tag{3.3}$$

The problem may then be reformulated in terms of the unknown potential ϕ_1.

To satisfy condition (3.2), the function ϕ_2 must take the form

$$\phi_2 = \frac{i}{k_1}\left(a_1 + \frac{a_2k_1 - a_1k_2}{1 + ia_0U_\infty k_1}\frac{1 - e^{-ik_2X_2}}{k_2}\right)e^{i\mathbf{k}\cdot(\mathbf{X}_e - i\mathbf{U}_\infty t)}, \tag{3.4}$$

where the vector $\mathbf{X}_e$ satisfies

$$|\mathbf{X}_e - \mathbf{X}| \to 0 \quad \text{as } r \to \infty. \tag{3.5}$$

Condition (3.5) must be satisfied to within $O(1/r^\nu)$, with $\nu > 1$, to ensure that ϕ_2 cancels $\tilde{\phi}$ as $r \to \infty$. This strict condition guarantees that ϕ_1 will have outgoing wave behavior at infinity. $\mathbf{X}_e$ is then defined as

$$X_{e,1} = \frac{\Phi_0}{U_\infty} - \frac{\Gamma}{\pi U_\infty}\operatorname{sgn}(\Psi_0)\left[\frac{\pi}{2} + \operatorname{sgn}(\Psi_0)\tan^{-1}\left(\frac{\rho_\infty\Phi_0}{\beta_\infty\Psi_0}\right)\right] \times [1 - e^{-(\Phi_0^2 + \Psi_0^2/\beta_\infty^2)(2/cU_\infty^2)}] \tag{3.6}$$

$$X_{e,2} = X_2 \tag{3.7}$$

$$X_{e,3} = X_3. \tag{3.8}$$

The expression for $X_{e,1}$ is obtained by making a far-field expansion of the drift function Δ in terms of Φ_0 and Ψ_0. (c is the airfoil chord length, and the parameter β_∞ is equal to $\sqrt{1 - M_\infty^2}$, where M_∞ is the free stream Mach number.) The first term in the expansion is just Φ_0/U_∞, whereas the second term arises due to the circulation around the airfoil. Since the second term vanishes for airfoils with zero lift, it is clear that the expression for ϕ_2 is much simpler for nonlifting airfoils than for lifting airfoils.

It should be noted that the first factor in brackets in Eq. (3.6) is discontinuous and undefined at the points on the airfoil, where $\Phi_0 = 0$, $\Psi_0 = 0^+$ and $\Phi_0 = 0$, $\Psi_0 = 0^-$. The second factor in brackets is not part of the expansion itself, but is included to remove the discontinuity in $X_{e,1}$. By including the second factor and defining $X_{e,1} = 0$ at $\Phi_0 = 0$, $\Psi_0 = 0$, we obtain an expression for $X_{e,1}$ which is everywhere continuous. This ensures that the airfoil boundary condition for ϕ_1 will be continuous. (See Eq. (3.10) below.) Finally, we point out that the β_∞ term arises due to a Gothert's rule correction on the far-field mean velocity so that the expression for $X_{e,1}$ is valid for both compressible and incompressible flows.

Before summarizing the reformulated boundary value problem, we nondimensionalize the dependent and independent variables as follows:

$x_1, x_2, x_3, X_1, X_2, X_3, X_{e,1}$	by $c/2$
Φ_0, Γ	by $(c/2)U_\infty$
Ψ_0	by $(c/2)\rho_\infty U_\infty$
U_0, c_0	by U_∞
ρ_0	by ρ_∞
p'	by $\rho_\infty U_\infty\lvert\mathbf{a}\rvert$
t, Δ	by $c/2U_\infty$
ω	by $2U_\infty/c$
k_1, k_2, k_3	by $2/c$
$\phi, \tilde{\phi}, \phi_1, \phi_2$	by $(c/2)\lvert\mathbf{a}\rvert$
$\mathbf{a}$	by $\lvert\mathbf{a}\rvert$.

The normalized wave number k_1, which is equal to $\omega c/2U_\infty$, where ω and U_∞ are the dimensional angular frequency and free stream velocity, respectively, is called the reduced frequency.

The governing equation for ϕ_1 is then

$$\frac{D_0}{Dt}\left(\frac{1}{c_0^2}\frac{D_0\phi_1}{Dt}\right) - \frac{1}{\rho_0}\nabla\cdot(\rho_0\nabla\phi_1) = \frac{1}{\rho_0}\nabla\cdot(\rho_0\mathbf{u}^{(R)}) + \frac{D_0}{Dt}\left(\frac{1}{c_0^2}\frac{D_0\phi_2}{Dt}\right) - \frac{1}{\rho_0}\nabla\cdot(\rho_0\nabla\phi_2) \tag{3.9}$$

and the boundary conditions are

$$\nabla\phi_1\cdot\mathbf{n} = \nabla\phi_2\cdot\mathbf{n} \quad \text{airfoil surface} \tag{3.10}$$

$$\frac{D_0}{Dt}[\Delta(\phi_1-\phi_2)] = 0 \quad \text{wake} \tag{3.11a}$$

$$\Delta[\nabla(\phi_1-\phi_2)\cdot\mathbf{n}] = 0 \quad \text{wake} \tag{3.11b}$$

$$\nabla\phi_1 \to 0 \quad x_1 \to -\infty. \tag{3.12}$$

The nondimensional expressions for the potential functions $\tilde{\phi}$ and ϕ_2, for the unsteady velocity and pressure, and for the upstream velocity disturbances are given by

$$\tilde{\phi} = \frac{i}{k_1}\left(a_1 + \frac{a_2k_1 - a_1k_2}{1+ia_0k_1}\frac{1-e^{-ik_2X_2}}{k_2}\right)e^{i\mathbf{k}\cdot\mathbf{X}-ik_1t} \tag{3.13}$$

$$\phi_2 = \frac{i}{k_1}\left(a_1 + \frac{a_2k_1 - a_1k_2}{1+ia_0k_1}\frac{1-e^{-ik_2X_2}}{k_2}\right)e^{i\mathbf{k}\cdot\mathbf{X}_e-ik_1t}, \tag{3.14}$$

where

$$X_1 = \Delta, \quad X_2 = X_{e,2} = \Psi_0, \quad X_3 = X_{e,3} = x_3 \tag{3.15}$$

$$X_{e,1} = \Phi_0 - \frac{\Gamma}{\pi}\operatorname{sgn}(\Psi_0)\left[\frac{\pi}{2} + \operatorname{sgn}(\Psi_0)\tan^{-1}\left(\frac{\Phi_0}{\beta_\infty\Psi_0}\right)\right] \times [1 - e^{-(\Phi_0^2+\Psi_0^2)}] \tag{3.16}$$

$$\mathbf{u}(\mathbf{x},t) = \mathbf{u}^{(R)} + \nabla(\phi_1 - \phi_2), \tag{3.17}$$

where

$$\mathbf{u}^{(R)} = [\nabla(\mathbf{a}\cdot\mathbf{X})]e^{i\mathbf{k}\cdot\mathbf{X}-ik_1t} + \nabla\tilde{\phi} \tag{3.18}$$

$$p' = -\rho_0(\mathbf{x})\frac{D_0(\phi_1-\phi_2)}{Dt} \tag{3.19}$$

$$\mathbf{u}_\infty = \nabla(\mathbf{a}\cdot\mathbf{X})e^{i\mathbf{k}\cdot\mathbf{X}-ik_1t}. \tag{3.20}$$

3.2. *Determination of Mean Potential Flow*

In order to obtain numerical solutions to Eq. (3.9) and its associated boundary conditions, one must first solve for the steady potential flow about the airfoil. This will in general require the use of a standard potential flow solver such as FLO36 [13].

However, an examination of Eqs. (3.13)–(3.18) indicates that the most natural choice of independent variables in which to solve Eq. (3.9) are Φ_0 and Ψ_0, the mean flow potential and stream functions. Since potential flow codes solve the steady problem in terms of the spatial coordinates x_1 and x_2, there is some difficulty in obtaining the steady solution as a function of Φ_0 and Ψ_0.

Another difficulty arises due to the fact that the grids used by steady flow solvers are not suitable for the unsteady calculation. As reported in Refs. [14, 15], accurate solution of Eq. (3.9) over a large range of flow conditions requires using grids which are determined as a function of both the reduced frequency k_1 and the free-stream Mach number M_∞. This means that in general it will be necessary to interpolate the solution from the steady grid onto the appropriate unsteady grid.

Because of the loss of accuracy that can result from such an interpolation process and, also, because of the need to know the mean flow as a function of Φ_0 and Ψ_0, an approximate analytical scheme that can obtain the compressible, subsonic flow about isolated airfoils was developed. The scheme is based on the idea that, except for a small inner region surrounding the airfoil, the flow gradients are not too large. Thus in the large outer region extending to infinity, the mean flow is essentially governed by a set of linear equations. As a result, one can use Gothert's rule, whereby the compressible flow about a given airfoil can be obtained from the incompressible flow about a similar airfoil.

If we let α_C, θ_C, and γ_C denote the angle of attack, thickness ratio, and camber ratio, respectively, of the given airfoil in a compressible flow, then the transformed airfoil for the incompressible flow field has angle of attack, thickness ratio, and camber ratio given by

$$\begin{aligned}\alpha_I &= \beta_\infty\,\alpha_C\\ \theta_I &= \beta_\infty\,\theta_C\\ \gamma_I &= \beta_\infty\,\gamma_C\end{aligned} \tag{3.21}$$

where I subscripts denote quantities from the incompressible flow field. Denoting the compressible velocity by $(U_\infty + u_C, v_C)$ at the point (x, y) and the incompressible velocity by $(U_\infty + u_I, v_I)$ at the point (x_I, y_I), the spatial coordinates and velocity in the compressible and incompressible planes are related by

$$x = x_I \tag{3.22a}$$

$$y = \frac{y_I}{\beta_\infty} \tag{3.22b}$$

and

$$u_C = \frac{u_I}{\beta_\infty^2} \tag{3.23a}$$

$$v_C = \frac{v_I}{\beta_\infty}. \tag{3.23b}$$

It is assumed here that the free-stream velocity U_∞ is aligned with the x axis and that the angle of attack, thickness ratio, and camber ratio of the airfoil are such that the perturbation velocities are small compared to U_∞. The potential and stream functions of the compressible flow field are then related to the potential and stream functions of the incompressible flow field by

$$\Phi_0 - U_\infty x = \frac{1}{\beta_\infty^2}(\Phi_I - U_\infty x_I) \tag{3.24a}$$

$$\Psi_0 - U_\infty y = \frac{1}{\beta_\infty}(\Psi_I - U_\infty y_I) \tag{3.24b}$$

Using (3.22), Eqs. (3.24) can be rewritten

$$\Phi_I - M_\infty^2 x_I U_\infty = \beta_\infty^2 \Phi_0 \tag{3.25a}$$

$$\Psi_I = \beta_\infty \Psi_0. \tag{3.25b}$$

The problem is then, given (Φ_0, Ψ_0), solve Eqs. (3.25) for (Φ_I, Ψ_I) and then use (3.22) and (3.23) to determine the spatial coordinates (x, y) and velocity components (u_C, v_C) of the compressible flow field. If this can be done, then we have the compressible flow field determined as a function of (Φ_0, Ψ_0). Note that this assumes that we can determine (x_I, y_I) and (u_I, v_I) as functions of (Φ_I, Ψ_I). Since there is a one-to-one correspondence between (x_I, y_I) and (Φ_I, Ψ_I), and between (u_I, v_I) and (Φ_I, Ψ_I), this is not a difficulty. At the least, it can always be done numerically. For the special case of Joukowski airfoils, however, it is possible to express the complex potential (Φ_I, Ψ_I) in terms of the polar coordinates (r, θ), and then obtain (x_I, y_I) and (u_I, v_I) through known functional expressions of (r, θ).

For the case of incompressible flow around a Joukowski airfoil the complex potential is given by

$$\Phi_I + i\Psi_I = U_\infty \zeta' + \frac{U_\infty a^2}{\zeta'} + \frac{\Gamma_I}{2\pi i} \ln\left(\frac{\zeta'}{a}\right) + K, \tag{3.26}$$

where K is an arbitrary constant and

$$\zeta' = (\zeta_I - \zeta_{0'})e^{-i\alpha} = re^{i\theta}. \tag{3.27}$$

Here $\zeta_{0'} = -\varepsilon + i\varepsilon'$ is a complex constant, and the parameters a, ε, and ε' depend on the airfoil geometry. Γ_I is the steady circulation around the airfoil and is given by

$$\Gamma_I = -4\pi a U_\infty \sin(\alpha_I + \beta), \tag{3.28}$$

where β is defined by

$$\sin\beta = \varepsilon'/a. \tag{3.29}$$

The spatial coordinates (x_I, y_I) are determined from r and θ through the Joukowski transformation

$$x_I + i y_I = \left(\zeta_I + \frac{d^2}{\zeta_I}\right)e^{-i\alpha}, \tag{3.30}$$

where the parameter d satisfies

$$(\varepsilon + d)^2 + \varepsilon'^2 = a^2. \tag{3.31}$$

Finally, the velocity components (u_I, v_I) are given by

$$u_I - i v_I = U_\infty \left[\frac{(\zeta' + \zeta_{0'}e^{-i\alpha_I})^2[\zeta' + ae^{i(\alpha_I+\beta)}]}{\zeta'^2[\zeta' + (\zeta_{0'} + d)e^{-i\alpha_I}]} - 1\right]. \tag{3.32}$$

Using (3.26)–(3.30), Eqs. (3.25) can be expressed in terms of r and θ as

$$\begin{aligned} &U_\infty\left(r + \frac{a^2}{r}\right)\cos(\theta - \alpha_I) - [2U_\infty a \sin(\alpha_I + \beta)]\theta + K \\ &\quad - M_\infty^2 U_\infty \left[r\cos\theta - \varepsilon\cos\alpha_I + \varepsilon'\sin\alpha_I \right. \\ &\quad \left. + \frac{d^2[(r\cos(\theta + 2\alpha_I) - \varepsilon\cos\alpha_I - \varepsilon'\sin\alpha_I]}{[r\cos(\theta + \alpha_I) - \varepsilon]^2 + [r\sin(\theta + \alpha_I) + \varepsilon']^2}\right] \\ &\quad = \beta_\infty^2 \Phi_0 \\ &U_\infty\left(r - \frac{a^2}{r}\right)\sin\theta + 2aU_\infty \sin(\alpha_I + \beta)\ln\left(\frac{r}{a}\right) = \beta_\infty \Psi_0. \end{aligned} \tag{3.33}$$

If for given Φ_0 and Ψ_0 we can solve Eqs. (3.33) for r and θ, then Eqs. (3.30) and (3.32) can be used to get (x_I, y_I) and (u_I, v_I), and Eqs. (3.22) and (3.23) can be used to obtain (x, y) and (u_c, v_c). Once we have obtained (u_c, v_c), the other mean flow quantities can then be obtained from Bernoulli's law for polytropic gases.

We note that, while the system of Eqs. (3.33) is highly nonlinear in the unknowns r and θ, it can be routinely solved by Newton iteration. Once a subroutine has been developed to solve Eqs. (3.33), the compressible steady flow around any Joukowski airfoil can be very efficiently obtained. In addition, the mean flow is obtained for arbitrary Φ_0 and Ψ_0, so that there is no restriction whatsoever on the particular grid that may be used for the unsteady calculation.

The only limitation in obtaining the mean potential flow by this particular approach is the underlying assumption that u_C and v_C must be small compared to U_∞. This means that the method will not give a good approximation in the inner region and particularly near the stagnation point where the perturbation velocities are of the same order of magnitude as U_∞. However,

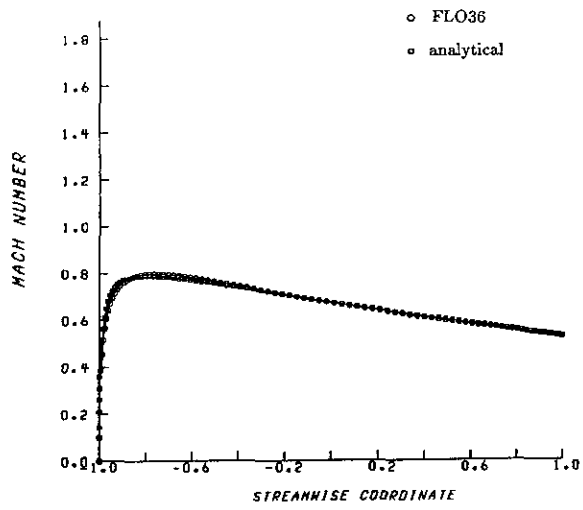

FIG. 1. Comparison of Mach number at the airfoil surface between FLO36 and the present analytical scheme. $M_\infty = 0.6$, $\alpha = 0°$, camber = 0, thickness = 0.12.

extensive testing of the present approach and comparing with the steady potential flow solver FLO36 has shown that the region of inaccuracy is very small. Figures 1 through 4 show Mach number comparisons between the present analytical scheme and FLO36. The comparison is made at grid points along fixed grid lines used by FLO36. It is seen that the agreement overall is quite good, with the exception of grid points on the airfoil surface that are near the stagnation point. Because of this inaccuracy, we use FLO36 to calculate the steady flow along the airfoil, and we use the analytical scheme off the airfoil, except in a small region just upstream of the stagnation point. In this region, for airfoils that have steady loading, the velocities are calculated using a Taylor series

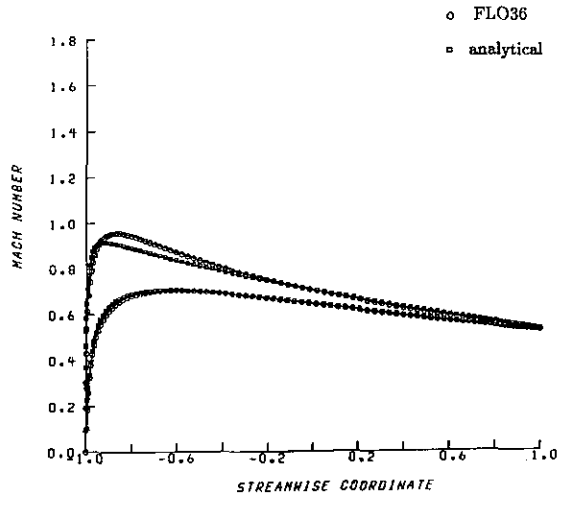

FIG. 2. Comparison of Mach number at the airfoil surface between FLO36 and the present analytical scheme. $M_\infty = 0.6$, $\alpha = 2°$, camber = 0, thickness = 0.12.

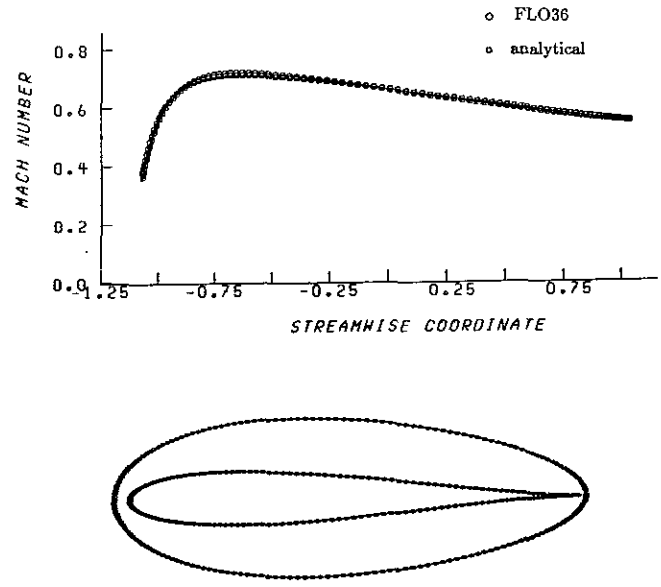

FIG. 3. Comparison of Mach number along a FLO36 grid line which wraps around the airfoil. $M_\infty = 0.6$, $\alpha = 0°$, camber = 0, thickness = 0.12.

expansion. For airfoils without steady loading, the velocities are calculated from a local analytical solution which is patched to the outer solution.

3.3. *Frequency Domain Formulation*

An inspection of Eqs. (3.13), (3.14), (3.18), and (3.20) indicates that the time dependence of the present boundary value

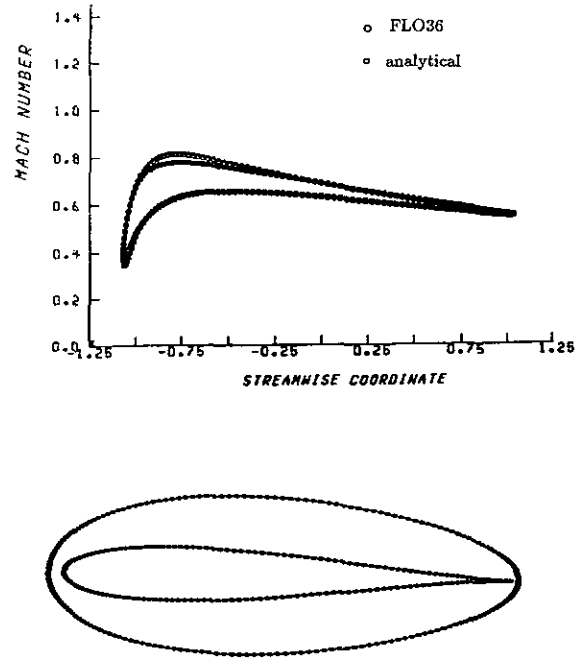

FIG. 4. Comparison of Mach number along a FLO36 grid line which wraps around the airfoil. $M_\infty = 0.6$, $\alpha = 2°$, camber = 0, thickness = 0.12.

problem comes entirely through the harmonic term $e^{-ik_1 t}$. It is therefore a simple matter to make a transformation from the time domain into the frequency domain. Such a transformation significantly reduces the mathematical complexity of the equations to be solved.

For the case of two-dimensional mean flow, we transform into the frequency domain with the following change of dependent variable:

$$\phi_1 = \varphi e^{-ik_1 t + ik_3 x_3}. \tag{3.34}$$

By including the $ik_3 x_3$ term in the transformation, the harmonic dependence on the spanwise component x_3 is also eliminated, since all of the $e^{ik_3 x_3}$ terms then factor out from each side of the equation. This is, of course, possible in view of (3.20) and (3.15).

To facilitate what follows, it is convenient to introduce the linear operators $\mathcal{L}$ and $\mathcal{L}_0$, where

$$\mathcal{L} = \frac{D_0}{Dt}\left(\frac{1}{c_0^2}\frac{D_0}{Dt}\right) - \frac{1}{\rho_0}\nabla\cdot(\rho_0\nabla) \tag{3.35}$$

$$\mathcal{L}_0 = M_\infty^2 \frac{D_0^2}{Dt_0^2} - \left(\frac{\partial^2}{\partial\Phi_0^2} + \frac{\partial^2}{\partial\Psi_0^2} + \frac{\partial^2}{\partial x_3^2}\right) \tag{3.36}$$

and where

$$\frac{D_0}{Dt_0} = \frac{\partial}{\partial t} + \frac{\partial}{\partial\Phi_0}. \tag{3.37}$$

The governing equation then takes the form

$$\mathcal{L}\phi_1 = \frac{1}{\rho_0}\nabla\cdot(\rho_0\mathbf{u}^{(R)}) + \mathcal{L}\phi_2. \tag{3.38}$$

The operator $\mathcal{L}_0$ is essentially the operator for the linear thin airfoil gust response problem. By writing the governing equation in the equivalent form shown in Eq. (3.39) below, the left-hand side of the equation will exhibit the character of the thin airfoil operator in the far field since $\mathcal{L} \to \mathcal{L}_0$ there,

$$\mathcal{L}_0\phi_1 + (\mathcal{L} - \mathcal{L}_0)\phi_1 = \frac{1}{\rho_0}\nabla\cdot(\rho_0\mathbf{u}^{(R)}) + \mathcal{L}\phi_2. \tag{3.39}$$

We then have in terms of φ

$$\begin{aligned}
&\mathcal{L}_0\phi_1 + (\mathcal{L} - \mathcal{L}_0)\phi_1 = e^{-ik_1 t + ik_3 x_3} \\
&\left\{ -\left[\beta_\infty^2 \frac{\partial^2\varphi}{\partial\Phi_0^2} + \frac{\partial^2\varphi}{\partial\Psi_0^2} + 2ik_1 M_\infty^2 \frac{\partial\varphi}{\partial\Phi_0} + (k_1^2 M_\infty^2 - k_3^2)\varphi\right]\right. \\
&\quad + \left[k_1^2 M_\infty^2 - \frac{k_1^2 M^2}{U_0^2} - ik_1 U_0^2 \frac{\partial}{\partial\Phi_0}\left(\frac{M^2}{U_0^2}\right)\right]\varphi \\
&\quad + \left[M^2\left(\frac{\partial U_0^2}{\partial\Phi_0} - 2ik_1\right) + 2ik_1 M_\infty^2\right. \\
&\quad + U_0^4 \frac{\partial}{\partial\Phi_0}\left(\frac{M^2}{U_0^2}\right) - \left.\frac{U_0^2}{\rho_0}\frac{\partial\rho_0}{\partial\Phi_0}\right]\frac{\partial\varphi}{\partial\Phi_0} \\
&\quad + (\beta_\infty^2 - \beta^2 U_0^2)\frac{\partial^2\varphi}{\partial\Phi_0^2} \\
&\quad \left. + (1 - U_0^2)\frac{\partial^2\varphi}{\partial\Psi_0^2} - \frac{U_0^2}{\rho_0}\frac{\partial\rho_0}{\partial\Psi_0}\frac{\partial\varphi}{\partial\Psi_0}\right\},
\end{aligned} \tag{3.40}$$

where M is the local Mach number of the mean flow, and $\beta^2 = 1 - M^2$.

Equation (3.40) may be simplified considerably by changing both the dependent and independent variables,

$$\varphi = \psi e^{-iK_0\Phi}, \tag{3.41a}$$

where

$$K_0 = k_1 M_\infty^2/\beta_\infty^2, \tag{3.41b}$$

and

$$\Phi = \Phi_0 \tag{3.42a}$$

$$\Psi = \beta_\infty \Psi_0. \tag{3.42b}$$

Expressing Eq. (3.40) in terms of ψ and the new independent variables Φ and Ψ, one gets

$$\begin{aligned}
&\mathcal{L}_0\phi_1 + (\mathcal{L} - \mathcal{L}_0)\phi_1 \\
&= e^{-ik_1 t + ik_3 x_3} e^{-iK_0\Phi}\left\{ -\beta_\infty^2\left[\frac{\partial^2\psi}{\partial\Phi^2} + \frac{\partial^2\psi}{\partial\Psi^2} + \left(\frac{k_1^2 M_\infty^2}{\beta_\infty^4} - \frac{k_3^2}{\beta_\infty^2}\right)\psi\right]\right. \\
&\quad \left. + A_1\psi + A_2\frac{\partial\psi}{\partial\Phi} + A_3\frac{\partial\psi}{\partial\Psi} + A_4\frac{\partial^2\psi}{\partial\Phi^2} + A_5\frac{\partial^2\psi}{\partial\Psi^2}\right\},
\end{aligned} \tag{3.43}$$

where $A_1 \cdots A_5$ are functions of (Φ,Ψ) defined by

$$\begin{aligned}
A_1(\Phi,\Psi) &= \frac{k_1^2 M_\infty^2}{\beta_\infty^2} - \frac{k_1^2 M^2}{U_0^2} - ik_1 U_0^2 \frac{\partial}{\partial\Phi}\left(\frac{M^2}{U_0^2}\right) \\
&\quad - iK_0\left[M^2\left(\frac{\partial U_0^2}{\partial\Phi} - 2ik_1\right) + U_0^4\frac{\partial}{\partial\Phi}\left(\frac{M^2}{U_0^2}\right)\right. \\
&\quad \left. - \frac{U_0^2}{\rho_0}\frac{\partial\rho_0}{\partial\Phi}\right] + \frac{k_1^2 M_\infty^4}{\beta_\infty^4}\beta^2 U_0^2
\end{aligned}$$

$$A_2(\Phi,\Psi) = M^2\left(\frac{\partial U_0^2}{\partial\Phi} - 2ik_1\right) + U_0^4\frac{\partial}{\partial\Phi}\left(\frac{M^2}{U_0^2}\right) \tag{3.44a}$$

$$- \frac{U_0^2}{\rho_0}\frac{\partial\rho_0}{\partial\Phi} + 2iK_0\beta^2 U_0^2 \tag{3.44b}$$

$$A_3(\Phi, \Psi) = -\frac{U_0^2}{\rho_0}\frac{\partial \rho_0}{\partial \Psi} \tag{3.44c}$$

$$A_4(\Phi, \Psi) = \beta_\infty^2 - \beta^2 U_0^2 \tag{3.44d}$$

$$A_5(\Phi, \Psi) = 1 - U_0^2. \tag{3.44e}$$

Note that in the far field the functions $A_1 \cdots A_5$ tend to zero so that the right-hand side of (3.43) reduces to that of the linear thin airfoil theory [16].

To complete the frequency domain formulation, it is necessary to derive the expressions corresponding to the right-hand side of Eq. (3.39). We will refer to the right-hand side of (3.39) as the source term and denote it by $e^{-ik_1 t + ik_3 x_3} S$. The governing equation then becomes

$$\mathcal{L}_0 \phi_1 + (\mathcal{L} - \mathcal{L}_0)\phi_1 = e^{-ik_1 t + ik_3 x_3} S \tag{3.45a}$$

or

$$\mathcal{L}_0 \phi_1 + (\mathcal{L} - \mathcal{L}_0)\phi_1 = e^{-ik_1 t + ik_3 x_3}(S_1 + S_2 + S_3 - S_4), \tag{3.45b}$$

where

$$e^{-ik_1 t + ik_3 x_3} S_1 = \frac{\nabla \rho_0}{\rho_0} \cdot \{[\nabla(\mathbf{a} \cdot \mathbf{X})] e^{i\mathbf{k}\cdot\mathbf{X} - ik_1 t} + \nabla \tilde{\phi}\} \tag{3.46a}$$

$$e^{-ik_1 t + ik_3 x_3} S_2 = \nabla \cdot \{[\nabla(\mathbf{a} \cdot \mathbf{X})] e^{i\mathbf{k}\cdot\mathbf{X} - ik_1 t} + \nabla \tilde{\phi}\} \tag{3.46b}$$

$$e^{-ik_1 t + ik_3 x_3} S_3 = \frac{D_0}{Dt}\left(\frac{1}{c_0^2}\frac{D_0 \phi_2}{Dt}\right) \tag{3.46c}$$

$$e^{-ik_1 t + ik_3 x_3} S_4 = \frac{1}{\rho_0} \nabla \cdot (\rho_0 \nabla \phi_2). \tag{3.46d}$$

The frequency domain governing equation is then given by

$$\begin{aligned} &-\beta_\infty^2 \left[\frac{\partial^2 \psi}{\partial \Phi^2} + \frac{\partial^2 \psi}{\partial \Psi^2} + \left(\frac{k_1^2 M_\infty^2}{\beta_\infty^4} - \frac{k_3^2}{\beta_\infty^2}\right)\psi\right] \\ &+ A_1 \psi + A_2 \frac{\partial \psi}{\partial \Phi} + A_3 \frac{\partial \psi}{\partial \Psi} + A_4 \frac{\partial^2 \psi}{\partial \Phi^2} + A_5 \frac{\partial^2 \psi}{\partial \Psi^2} \\ &= e^{iK_0 \Phi}(S_1 + S_2 + S_3 - S_4), \end{aligned} \tag{3.47}$$

where $A_1 \cdots A_5$ are defined by Eqs. (3.44) and $S_1 \cdots S_4$ are defined by Eqs. (3.46). In the far field both the coefficients $A_1 \cdots A_5$ and the source term $S_1 + S_2 + S_3 - S_4$ tend to zero so that the equation reduces to a Helmholtz equation.

We conclude this section by presenting the frequency domain formulation of the airfoil and wake boundary conditions. The airfoil boundary condition, Eq. (3.10), becomes

$$\frac{\partial \psi}{\partial \Psi} = -\frac{e^{iK_0 \Phi}}{\beta_\infty}\left[\frac{a_1 \beta_\infty \Gamma}{\pi}\frac{1 - e^{-\Phi^2}}{\Phi} + \frac{a_2 + i a_0 a_1 k_2}{1 + i a_0 k_1}\right] e^{ik_1 X_{e,1}}. \tag{3.48}$$

The wake boundary condition (3.11a) is given by

$$\left(-ik_1 + U_0^2 \frac{\partial}{\partial \Phi}\right)[\triangle(\psi e^{-iK_0 \Phi} - \varphi_2)] = 0, \tag{3.49a}$$

where

$$e^{-ik_1 t + ik_3 x_3} \varphi_2 = \phi_2 \tag{3.49b}$$

and where $\triangle(\psi e^{-iK_0 \Phi} - \varphi_2)$ denotes the jump in the quantity $(\psi e^{-iK_0 \Phi} - \varphi_2)$ across the vortex sheet behind the airfoil. Finally, condition (3.11b) becomes

$$\triangle[\nabla(\psi e^{-iK_0 \Phi} - \varphi_2) \cdot \mathbf{n}] = 0. \tag{3.49c}$$

3.4. *Transformation into Computational Coordinates*

Previous experience in solving Eq. (3.47) for the case of flat plate and symmetric airfoils has shown that the independent variables (Φ, Ψ) are not suitable computational coordinates for the gust response problem [14, 15]. There are difficulties in obtaining consistently accurate results over a large range of Mach numbers and reduced frequencies, and also problems with the implementation of far-field boundary conditions. To remedy these difficulties, we transform into the computational coordinates (η, ξ) with the elliptic coordinate transformation

$$\Phi = a^* \cos(\pi \eta) \cosh(\pi \xi) \tag{3.50a}$$

$$\Psi = a^* \sin(\pi \eta) \sinh(\pi \xi), \tag{3.50b}$$

where a^* is an arbitrary constant which will be defined later. Note that in the far field the elliptic coordinates reduce essentially to cylindrical coordinates and that the Φ–Ψ plane is mapped into a semi-infinite strip in the η–ξ plane.

With this change of variables, the governing equation becomes

$$\begin{aligned} &-\beta_\infty^2 \left[\frac{\partial^2 \psi}{\partial \eta^2} + \frac{\partial^2 \psi}{\partial \xi^2} + J(\eta, \xi)\left(\frac{k_1^2 M_\infty^2}{\beta_\infty^4} - \frac{k_3^2}{\beta_\infty^2}\right)\psi\right] \\ &+ A_1 J(\eta, \xi)\psi + T_1 \frac{\partial \psi}{\partial \xi} + T_2 \frac{\partial \psi}{\partial \eta} + T_3 \frac{\partial^2 \psi}{\partial \xi^2} + T_4 \frac{\partial^2 \psi}{\partial \eta^2} \\ &+ T_5 \frac{\partial^2 \psi}{\partial \eta \partial \xi} = e^{iK_0 \Phi}(S_1 + S_2 + S_3 - S_4) J(\eta, \xi). \end{aligned} \tag{3.51}$$

Here $J(\eta, \xi)$ is the Jacobian of the transformation (3.50) and is given by

$$J(\eta, \xi) = \pi^2 a^{*2}[\sin^2(\pi\eta) + \sinh^2(\pi\xi)]. \tag{3.52}$$

Each of the T_i coefficients are known functions of η and ξ.

To complete the formulation of the numerical boundary value problem, the boundary conditions must also be specified in terms of the variables η and ξ.

The airfoil boundary condition, Eq. (3.48), becomes

$$\frac{\partial \psi}{\partial \xi} = -a^*\pi \sin(\pi\eta)\frac{e^{iK_0\Phi}}{\beta_\infty} \left[\frac{a_1\beta_\infty\Gamma}{\pi}\frac{1 - e^{-\Phi^2}}{\Phi} + \frac{a_2 + ia_0a_1k_2}{1 + ia_0k_1}\right]e^{ik_1X_{e,1}}. \tag{3.53}$$

Equation (3.49a), which specifies continuity of pressure across the wake, may be integrated to obtain

$$\Delta(\psi e^{-iK_0\Phi}) = \Delta\varphi_2 + [\Delta(\psi e^{-iK_0\Phi})_{\text{t.e.}} - \Delta\varphi_{2_{\text{t.e.}}}]e^{[ik_1\int_{\Phi_{\text{t.e.}}}^{\Phi}(d\Phi/U_0)]}, \tag{3.54}$$

where the subscript t.e. denotes quantities at the airfoil trailing edge. In general, both ψ and Φ are discontinuous across the wake. Hence, in evaluating $\Delta(\psi e^{-iK_0\Phi})$, one must account for the jump in both ψ and Φ.

Condition (3.49c), which specifies continuity of normal velocity across the wake, may be written

$$\left[U_0\frac{\partial}{\partial\Psi}(\psi e^{-iK_0\Phi} - \varphi_2)\right]^+ = \left[U_0\frac{\partial}{\partial\Psi}(\psi e^{-iK_0\Phi} - \varphi_2)\right]^-, \tag{3.55}$$

where "+" and "−" superscripts denote above and below the wake, respectively, and the derivatives in (3.55) are taken to be one-sided.

To express (3.54) and (3.55) in terms of η and ξ, it is necessary to first discuss in more detail the mapping defined by (3.50). First, the constant a^* is determined from the condition that the airfoil trailing edge point on the suction side, where $\Phi = a^*$, $\Psi = 0$, should map into the point $\eta = 0$, $\xi = 0$, and the stagnation point, where $\Phi = -a^*$, $\Psi = 0$ should map into the point $\eta = 1$, $\xi = 0$. Then a^* must be determined from

$$a^* = \frac{1}{2}\int_{\text{t.e.}}^{\text{s.p.}} U_0 ds \tag{3.56}$$

where s denotes arc length along the airfoil surface, t.e. denotes the airfoil trailing edge, and s.p. denotes the stagnation point. The steady solver FLO36 is used to locate the stagnation point, and then (3.56) is integrated numerically.

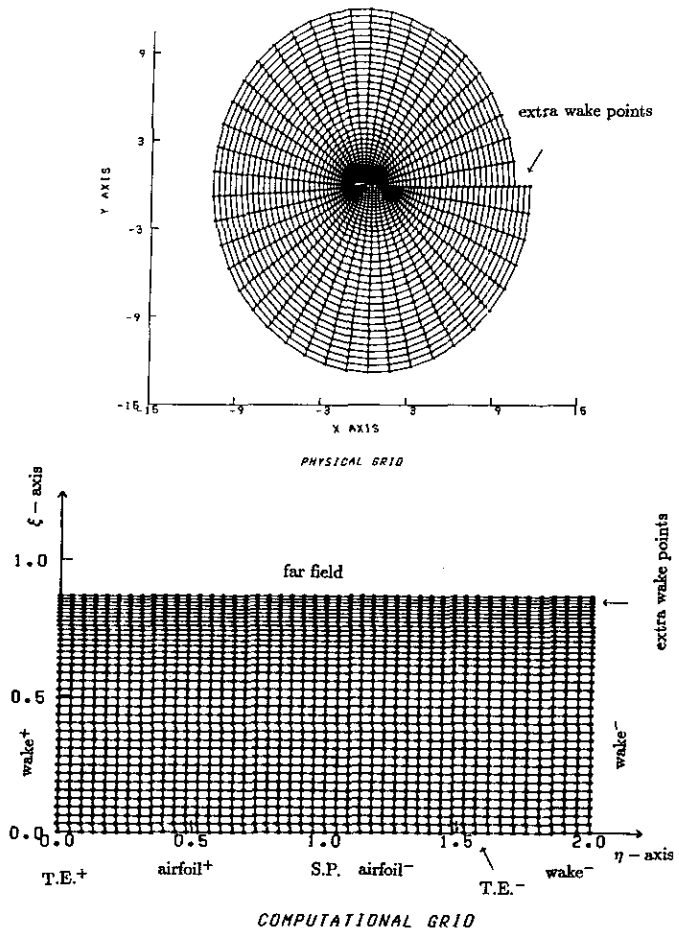

FIG. 5. Computational and physical grids.

With a^* defined by (3.56), the suction surface of the airfoil corresponds to the line segment on the η axis between 0 and 1. The pressure surface corresponds to the line segment on the η axis between 1 and $\eta_{\text{t.e.}-}$, where $\eta_{\text{t.e.}-} < 2.0$ (see Fig. 5). The pressure side of the wake is given by the two line segments $\{\eta_{\text{t.e.}-} < \eta \leq 2.0, \xi = 0\}$, and $\{\eta = 2.0, \xi > 0\}$. The suction side of the wake is represented by the positive ξ axis. The upper boundary of the η–ξ grid, which is given by $\{\xi = \xi_{\max}, 0 \leq \eta \leq 2\}$, corresponds to the far-field boundary.

Because of the discontinuity in Φ across the wake, the upper and lower surface wake grid points do not coincide. This presents some difficulty in the implementation of boundary conditions (3.54) and (3.55), since these conditions both specify a relation that must be satisfied across the wake. The difficulty

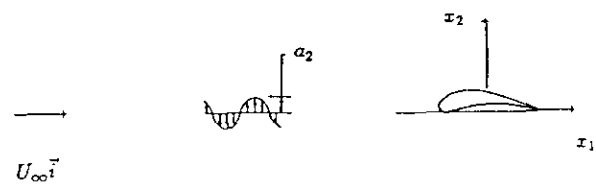

FIG. 6. Airfoil in a transverse gust.

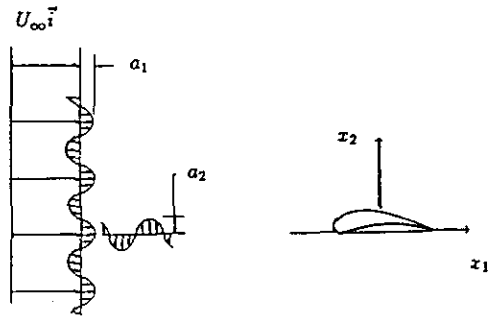

FIG. 7. Airfoil in a transverse and longitudinal gust.

can be removed, however, by simply using a linear averaging of ψ at two adjacent grid points to represent ψ at an arbitrary point in between. Using such a linear averaging, boundary condition (3.54), which is imposed for wake grid points on the pressure side, becomes

$$[(\psi e^{-iK_0\Phi})]^+_{\text{avg}} - [(\psi e^{-iK_0\Phi})]^- = \Delta\varphi_2 + [\Delta(\psi e^{-iK_0\Phi})_{\text{t.e.}} - \Delta\varphi_{2_{\text{t.e.}}}] e^{[ik_1 \int_{\Phi_{\text{t.e.}}}^{\Phi} (d\Phi/U_0^+)]}. \tag{3.57}$$

The discontinuity in Φ across the wake also leads to a shift in the location of the corresponding grid points in the physical plane on opposite sides of the wake. Because of this shift, the last several grid points on the pressure side in the physical plane extend past the last suction side wake grid point, so that condition (3.57) cannot be imposed. (see Fig. 5). However, because these last few points are in the far field where the mean flow is nearly uniform, the function ψ behaves essentially as in the case of the thin airfoil and is approximately an odd

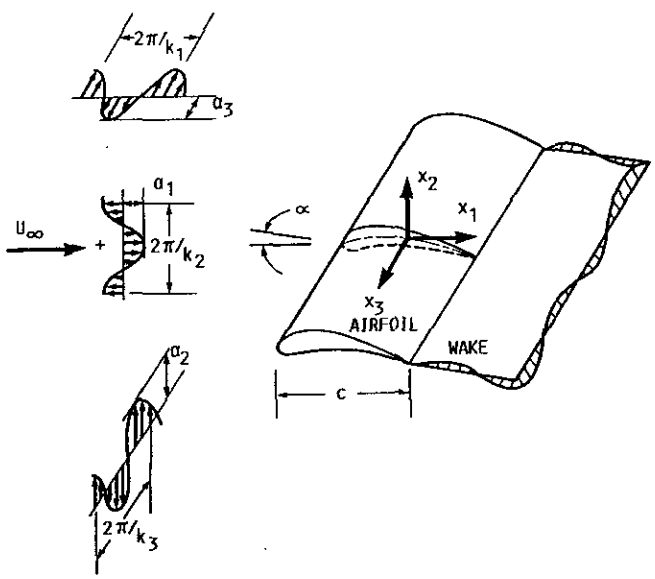

FIG. 8. Airfoil in a three-dimensional gust.

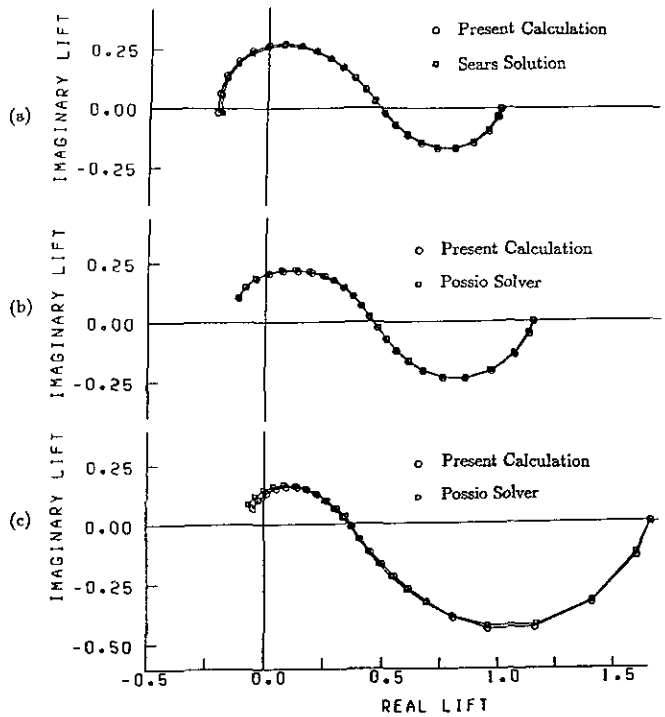

FIG. 9. Comparison between the numerically computed unsteady lift and analytical results for a flat plate airfoil in a transverse gust at (a) $M = 0.1$, (b) $M = 0.5$, and (c) $M = 0.8$; $k_1 = 0.0$, 0.007, 0.027, 0.062, 0.110, 0.172, 0.248, 0.338, 0.442, 0.561, 0.694, 0.842, 1.01, 1.18, 1.38, 1.59, 1.82, 2.07, 2.33, 2.62, 2.93, 3.26, 3.62, 4.01.

function of Ψ. By assuming ψ to be an odd function in this region, condition (3.54) becomes

$$[(\psi e^{-iK_0\Phi})]^- = -\frac{1}{2}\Delta\varphi_2 - \frac{1}{2}[\Delta(\psi e^{-iK_0\Phi})_{\text{t.e.}} - \Delta\varphi_{2_{\text{t.e.}}}] e^{[ik_1 \int_{\Phi_{\text{t.e.}}}^{\Phi} (d\Phi/U_0^+)]}. \tag{3.58}$$

This condition is imposed for extra far-field wake grid points on the pressure side.

For wake grid points on the suction side, we impose condition (3.55). Using linear averaging, this becomes

$$\left[U_0 \frac{\partial}{\partial\Psi}(\psi e^{-iK_0\Phi} - \varphi_2)\right]^+ = [U_0 \frac{\partial}{\partial\Psi}(\psi e^{-iK_0\Phi} - \varphi_2)]^-_{\text{avg}}. \tag{3.59}$$

Expressing this in η and ξ, one gets

$$\left[e^{-iK_0\Phi} \frac{U_0}{\sinh(\pi\xi)} \frac{\partial\psi}{\partial\eta}\right]^+ - \left[e^{-iK_0\Phi} \frac{U_0}{\sin(\pi\eta)} \frac{\partial\psi}{\partial\xi}\right]^-_{\text{avg}} = U_0^+ \left(\frac{\partial\varphi_2^+}{\partial\Psi} - \frac{\partial\varphi_2^-}{\partial\Psi}\right) \tag{3.60}$$

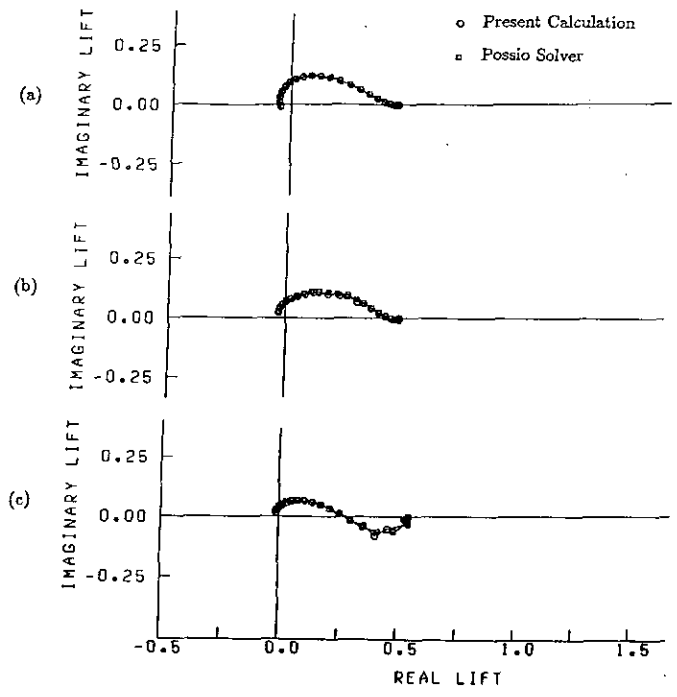

FIG. 10. Comparison between the numerically computed unsteady lift and analytical results for a flat plate airfoil in a three-dimensional gust at (a) $M = 0.1$, (b) $M = 0.5$, and (c) $M = 0.8$; $k_3 = 0.442$, $|\mathbf{a}| = 1$, $a_2/a_1 = -7/4$, $k_1 = k_2$, $\mathbf{a} \cdot \mathbf{k} = 0$, $a_2 > 0$; $k_1 = 0.0, 0.007, 0.027, 0.062, 0.110, 0.172, 0.248, 0.338, 0.442, 0.561, 0.694, 0.842, 1.01, 1.18, 1.38, 1.59, 1.82, 2.07, 2.33, 2.62, 2.93, 3.26, 3.62, 4.01$.

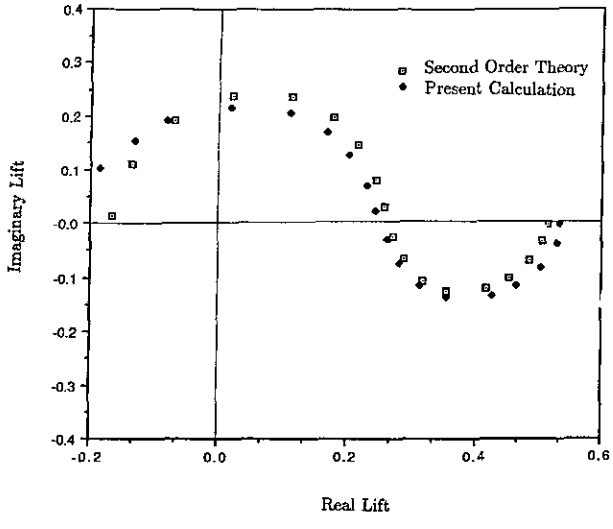

FIG. 11. Comparison between the numerically computed unsteady lift and the second-order theory for an airfoil in a transverse and longitudinal gust. The second-order theory does not account for the thickness of the airfoil. $M = 0.1$, $\alpha = 2°$, camber = 0.05, thickness ratio = 0.06; $-a_1 = a_2 = 0.7071$, $k_1 = k_2$, $a_3 = k_3 = 0$; $k_1 = 0.0, 0.01, 0.03, 0.06, 0.1, 0.2, 0.3, 0.45, 0.6, 0.8, 1.0, 1.3, 1.6, 2.0, 2.5, 3.0, 3.5, 4.0$.

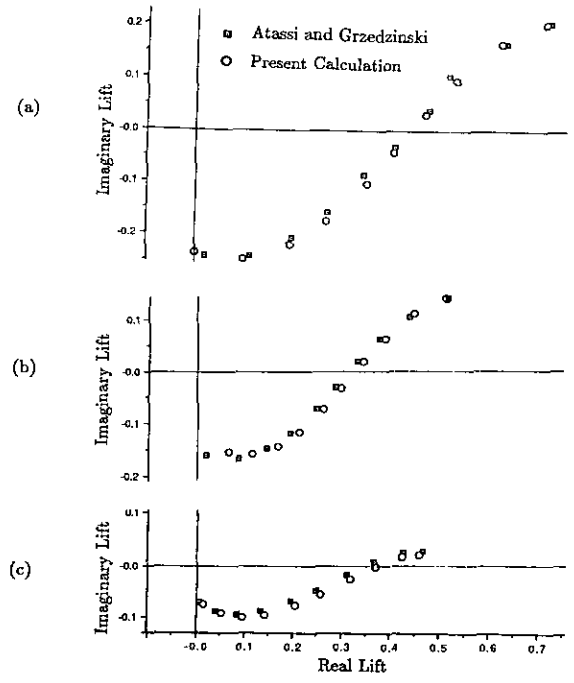

FIG. 12. Comparison between the numerically computed unsteady lift and the first order results of Atassi and Grzedzinski for (a) a transverse gust, (b) a transverse and longitudinal gust with $-a_1 = a_2 = 0.7071$, $k_1 = k_2$, $a_3 = k_3 = 0$, and (c) a three-dimensional gust with $k_3 = 0.4$, $|\mathbf{a}| = 1$, $a_2/a_1 = -7/4$, $k_1 = k_2$, $\mathbf{a} \cdot \mathbf{k} = 0$, $a_2 > 0$. $M_\infty = 0.1$, $\alpha = 0$, camber = 0, thickness ratio = 0.12. Results shown are the complex conjugate values of the unsteady lift; $k_1 = 0.2, 0.3, 0.45, 0.6, 0.8, 1.0, 1.3, 1.6, 2.0, 2.5$.

when the averaged values of ψ lie on the η axis. When the averaged values of ψ lie on the right-hand boundary of the η–ξ grid $\{\eta = 2.0, \xi > 0\}$, (3.59) becomes

$$\left[e^{-iK_0\Phi}\frac{U_0}{\sinh(\pi\xi)}\frac{\partial\psi}{\partial\eta}\right]^{+} - \left[e^{-iK_0\Phi}\frac{U_0}{\sinh(\pi\xi)}\frac{\partial\psi}{\partial\eta}\right]^{-}_{\text{avg}} = U_0^{+}\left(\frac{\partial\varphi_2^{+}}{\partial\Psi} - \frac{\partial\varphi_2^{-}}{\partial\Psi}\right). \tag{3.61}$$

Boundary conditions must also be specified at the airfoil trailing edge. At the upper trailing edge point, corresponding to $(\eta, \xi) = (0, 0)$, the Jacobian of the coordinate transformation (3.50) vanishes. Requiring the velocity to be finite at this point, (i.e., imposing the Kutta condition), we are led to

$$\frac{\partial\psi}{\partial\eta} = 0 \quad \text{at } (\eta, \xi) = (0, 0). \tag{3.62}$$

At the lower trailing edge point, we require the pressure to be continuous,

$$p'_{\text{t.e.}+} = p'_{\text{t.e.}-} \quad \text{at } (\eta, \xi) = (\eta_{\text{t.e.}-}, 0). \tag{3.63}$$

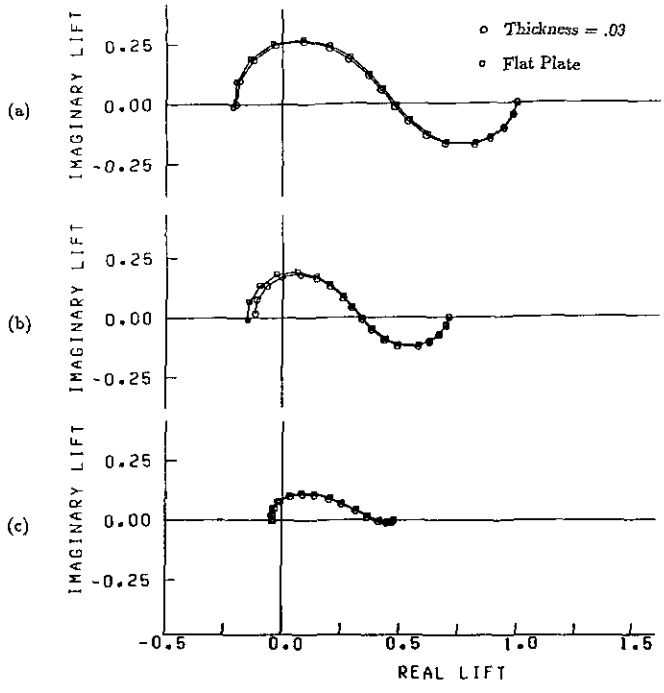

FIG. 13. Comparison between the unsteady lift of a flat plate airfoil and a 3% thick Joukowski airfoil in (a) a transverse gust, (b) a transverse and longitudinal gust with $-a_1 = a_2 = 0.7071$, $k_1 = k_2$, $a_3 = k_3 = 0$, and (c) a three-dimensional gust with $k_3 = 0.4$, $|\mathbf{a}| = 1$, $a_2/a_1 = -7/4$, $k_1 = k_2$, $\mathbf{a} \cdot \mathbf{k} = 0$, $a_2 > 0$. $M_\infty = 0.1$, $\alpha = 0$, camber = 0. $k_1 = 0.0, 0.01, 0.03, 0.06, 0.1, 0.2, 0.3, 0.45, 0.6, 0.8, 1.0, 1.3, 1.6, 2.0, 2.5, 3.0, 3.5, 4.0$.

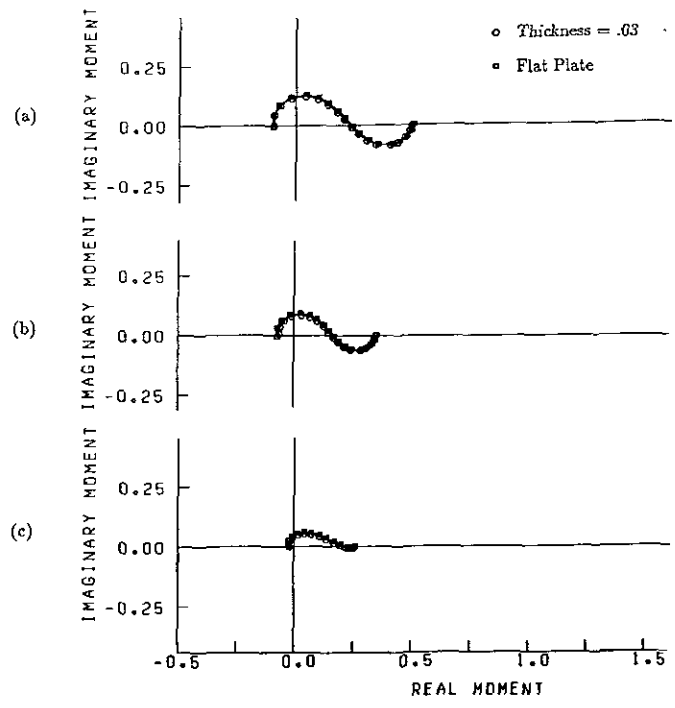

FIG. 14. Comparison between the unsteady moment of a flat plate airfoil and a 3% thick Joukowski airfoil in (a) a transverse gust, (b) a transverse and longitudinal gust with $-a_1 = a_2 = 0.7071$, $k_1 = k_2$, $a_3 = k_3 = 0$, and (c) a three-dimensional gust with $k_3 = 0.4$, $|\mathbf{a}| = 1$, $a_2/a_1 = -7/4$, $k_1 = k_2$, $\mathbf{a} \cdot \mathbf{k} = 0$, $a_2 > 0$. $M_\infty = 0.1$, $\alpha = 0$, camber = 0. $k_1 = 0.0, 0.01, 0.03, 0.06, 0.1, 0.2, 0.3, 0.45, 0.6, 0.8, 1.0, 1.3, 1.6, 2.0, 2.5, 3.0, 3.5, 4.0$.

Since the Jacobian vanishes at $(\eta, \xi) = (0, 0)$, it is not possible to directly calculate p' at that point. However, it can be approximated using a Taylor series expansion from neighboring points. Condition (3.63) can then be approximately satisfied.

Finally, one must impose a far-field boundary condition. Note that the function ϕ_1 was constructed so that it has outgoing wave behavior at infinity (see (3.1)–(3.8)). However, while condition (3.12) expresses the mathematical requirement that $\nabla\phi_1 \to 0$ at upstream infinity, this condition cannot be imposed throughout the far field on a boundary at a finite distance from the airfoil. Such a condition is a reflecting boundary condition which will not allow outgoing acoustic waves to exit the computational domain. A nonreflecting boundary condition must be used instead. Such a condition may be derived in a variety of ways. For example, by using separation of variables, one may derive a series solution for ψ in the far field. By accepting only those terms in the series which represent outgoing waves, one obtains a nonreflecting representation of the solution. However, when solving for the unknown coefficients of the series, one is led to a matrix which may not be sparse and which may also require pivoting and, therefore, longer solution times. In addition, since ψ is not continuous across the wake, but the series expansion for ψ is continuous everywhere, there is an incompatibility near the wake which can lead to a poor solution in the far field.

An alternative to the series expansion approach is to use a Sommerfeld radiation condition on the unsteady pressure. This approach avoids both the difficulties associated with the series expansion method and is also easier to implement. In the authors' experience, the Sommerfeld radiation condition has provided the most accurate, robust, and efficient far-field boundary condition for the gust response problem. In the present formulation, this condition may be written in operator notation as

$$\left[\frac{\partial}{\partial R} - i\sqrt{(k_1 M_\infty/\beta_\infty^2)^2 - (k_3/\beta_\infty)^2}\right]\left(\frac{\partial}{\partial \Phi} - i\frac{k_1}{\beta_\infty^2}\right)\psi = 0, \tag{3.64}$$

where

$$\Phi = R\cos\Theta \tag{3.65a}$$

$$\Psi = R\sin\Theta. \tag{3.65b}$$

Neglecting $(1/R)(\partial/\partial\Theta)$ terms, this reduces to

$$\cos\Theta\frac{\partial^2\psi}{\partial R^2} - i\left[\sqrt{(k_1 M_\infty/\beta_\infty^2)^2 - (k_3/\beta_\infty)^2}\cos\Theta + \frac{k_1}{\beta_\infty^2}\right]\frac{\partial\psi}{\partial R} - \frac{k_1}{\beta_\infty^2}\left[\sqrt{(k_1 M_\infty/\beta_\infty^2)^2 - (k_3/\beta_\infty)^2}\right]\psi = 0. \tag{3.66}$$

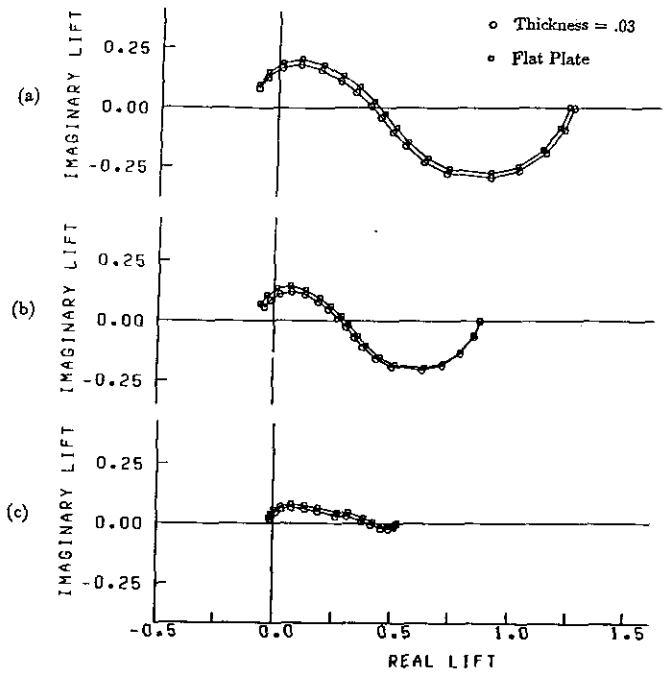

FIG. 15. Comparison between the unsteady lift of a flat plate airfoil and a 3% thick Joukowski airfoil in (a) a transverse gust, (b) a transverse and longitudinal gust with $-a_1 = a_2 = 0.7071$, $k_1 = k_2$, $a_3 = k_3 = 0$, and (c) a three-dimensional gust with $k_3 = 0.4$, $|\mathbf{a}| = 1$, $a_2/a_1 = -7/4$, $k_1 = k_2$, $\mathbf{a} \cdot \mathbf{k} = 0$, $a_2 > 0$. $M_\infty = 0.6$, $\alpha = 0$, camber = 0. $k_1 = 0.0, 0.01, 0.03, 0.06, 0.1, 0.2, 0.3, 0.45, 0.6, 0.8, 1.0, 1.3, 1.6, 2.0, 2.5, 3.0, 3.5, 4.0$.

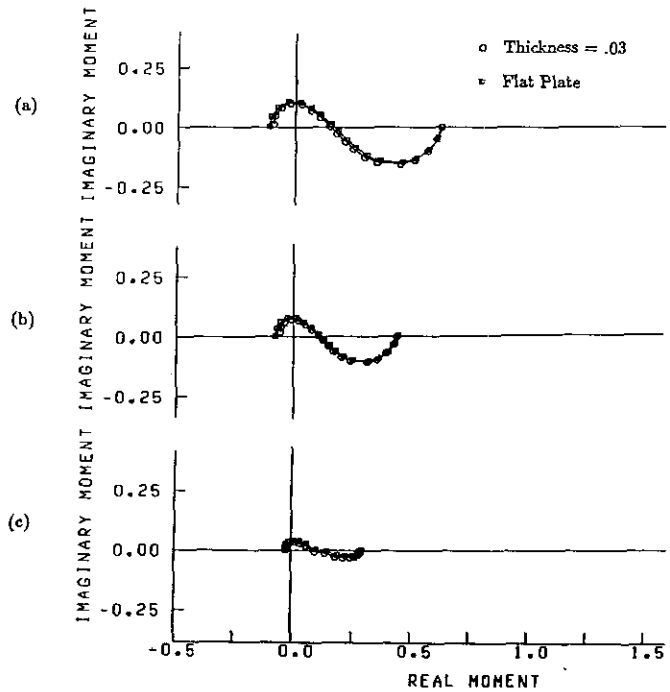

FIG. 16. Comparison between the unsteady moment of a flat plate airfoil and a 3% thick Joukowski airfoil in (a) a transverse gust, (b) a transverse and longitudinal gust with $-a_1 = a_2 = 0.7071$, $k_1 = k_2$, $a_3 = k_3 = 0$, and (c) a three-dimensional gust with $k_3 = 0.4$, $|\mathbf{a}| = 1$, $a_2/a_1 = -7/4$, $k_1 = k_2$, $\mathbf{a} \cdot \mathbf{k} = 0$, $a_2 > 0$. $M_\infty = 0.6$, $\alpha = 0$, camber = 0. $k_1 = 0.0, 0.01, 0.03, 0.06, 0.1, 0.2, 0.3, 0.45, 0.6, 0.8, 1.0, 1.3, 1.6, 2.0, 2.5, 3.0, 3.5, 4.0$.

This condition is applied for all grid points such that $0 < \eta < 2$, $\xi = \xi_{\max}$.

3.5. *Numerical Method*

The numerical boundary value problem consists of the governing equation (3.51) together with boundary conditions (3.53), (3.57), (3.58), (3.60), (3.61), (3.62), (3.63), and (3.66). Each equation can be expressed in discrete form by employing finite difference approximations.

The first step in obtaining numerical solutions is to calculate the source term S. It has been the authors' experience that a careful evaluation of the source term is required if accurate solutions to the gust response problem are to be obtained. This in turn depends largely upon the accurate evaluation of the drift function. By using the approximate analytical scheme outlined in Section 3.2, one can determine the mean velocities at arbitrary (Φ, Ψ). This means that for fixed Ψ, i.e., on a given streamline, we can determine the mean velocities for arbitrary Φ. Since evaluation of the drift function requires the integration of the expression $(1/U_0^2 - 1/U_\infty^2)$ with respect to Φ on a fixed streamline, the present approach greatly facilitates the accurate evaluation of the drift function Δ.

We evaluate Δ at a given grid point as the sum of an analytically determined part and a numerically determined part. The analytical part comes from a far-field expansion for Δ which is given by,

$$\Delta = \Phi_0 - \frac{\Gamma}{\pi}\operatorname{sgn}(\Psi_0)\left[\frac{\pi}{2} + \operatorname{sgn}(\Psi_0)\tan^{-1}\left(\frac{\Phi_0}{\beta_\infty \Psi_0}\right)\right]. \quad (3.67)$$

This expression can be used to determine Δ at some point far upstream, and then since Δ is additive, the remaining portion of the integration can be done numerically from the upstream location to the given grid point. The numerical integration is performed using the trapezoid rule with variable spacing in Φ to ensure accurate resolution near the airfoil. The first and second partial derivatives of Δ are approximated using four-point differencing.

Our discrete representation of the governing equation (3.51) employs the standard nine-point, central difference computational molecule which is second-order accurate in η and ξ. We assume that the spacing in each direction is nonuniform. Details of the grid spacing will be discussed momentarily. Each of the boundary conditions (3.53), (3.62), (3.63), and (3.66) are implemented using four-point, one-sided differencing which is third-order accurate for (3.53), (3.62), and (3.63), and second-order accurate for (3.66). Boundary conditions (3.60) and (3.61)

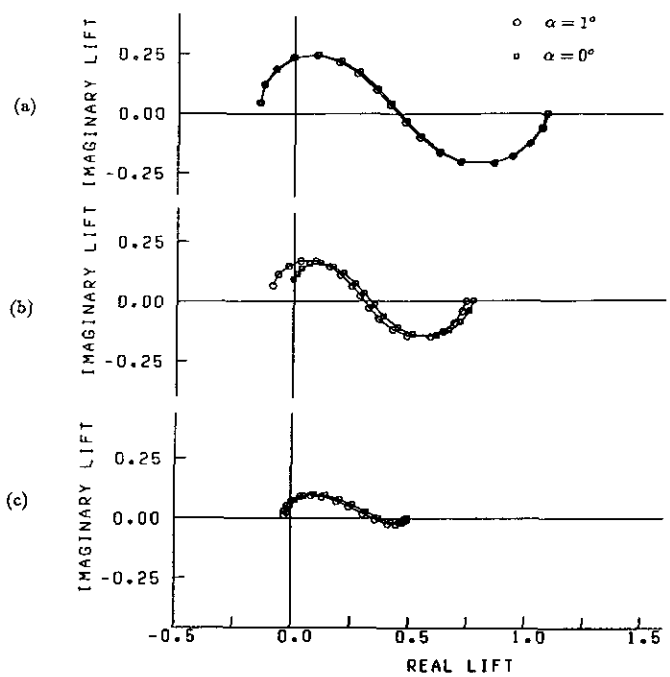

. FIG. 17. Comparison between the unsteady lift of a 12% thick, Joukowski airfoil at 0° angle of attack and 1° angle of attack for (a) a transverse gust, (b) a transverse and longitudinal gust with $-a_1 = a_2 = 0.7071$, $k_1 = k_2$, $a_3 = k_3 = 0$, and (c) a three-dimensional gust with $k_3 = 0.4$, $|\mathbf{a}| = 1$, $a_2/a_1 = -7/4$, $k_1 = k_2$, $\mathbf{a} \cdot \mathbf{k} = 0$, $a_2 > 0$. $M_\infty = 0.1$, camber = 0, thickness ratio = 0.12. $k_1 = 0.0, 0.01, 0.03, 0.06, 0.1, 0.2, 0.3, 0.45, 0.6, 0.8, 1.0, 1.3, 1.6, 2.0, 2.5, 3.0, 3.5, 4.0$.

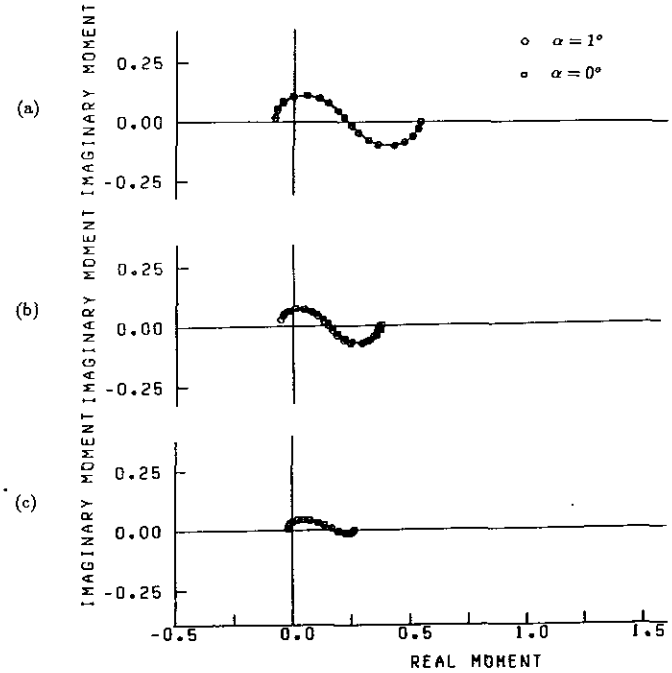

FIG. 18. Comparison between the unsteady moment of a 12% thick, Joukowski airfoil at 0° angle of attack and 1° angle of attack for (a) a transverse gust, (b) a transverse and longitudinal gust with $-a_1 = a_2 = 0.7071$, $k_1 = k_2$, $a_3 = k_3 = 0$, and (c) a three-dimensional gust with $k_3 = 0.4$, $|\mathbf{a}| = 1$, $a_2/a_1 = -7/4$, $k_1 = k_2$, $\mathbf{a} \cdot \mathbf{k} = 0$, $a_2 > 0$. $M_\infty = 0.1$, camber = 0, thickness ratio = 0.12. $k_1 = 0.0, 0.01, 0.03, 0.06, 0.1, 0.2, 0.3, 0.45, 0.6, 0.8, 1.0, 1.3, 1.6, 2.0, 2.5, 3.0, 3.5, 4.0$.

are both implemented using three-point, one-sided differencing which is second-order accurate.

Obtaining a numerical solution to the discrete system of finite-difference equations requires solving a complex variable matrix equation whose size is equal to the number of mesh points. It turns out, however, that there are difficulties in solving this linear system of equations because the matrix does not have a regular block structure which can be exploited. In addition, our experience has been that iterative solvers have convergence problems because the diagonal dominance of the matrix changes as the parameters M_∞, k_1, and k_3 are varied.

Because of these difficulties, we developed a general purpose, complex variable, direct sparse matrix solver. The solver basically works by using an ordered list to represent the nonzero entries of each row in the matrix and then inserts and deletes new entries in the matrix as multiples of each row are added to other rows to carry out the elimination process. The only requirement for the solver to work is that the matrix must remain reasonably sparse as the elimination is carried out. Pivoting during the elimination proved to be unnecessary.

The final issue to be discussed in regard to our numerical scheme is the method of grid determination. As reported previously [14, 15], it is not possible to use a single grid and obtain accurate solutions to the gust response problem for a large range of reduced frequencies. Rather, the unsteady grid must be determined as a function of both the mean flow Mach number and the reduced frequency.

This requirement is dictated by both the accuracy of the far-field boundary condition and the need to adequately model the airfoil and wake boundary conditions. It can be shown that the accuracy of the far-field condition (3.66) depends on the reduced frequency k_1 and free stream Mach number M_∞ in such a way that the parameter $(k_1 M_\infty/\beta_\infty^2) R^{3/2}$, where R is the distance to the far-field boundary, should remain large (compared to one) [17]. This shows that the location of the outer boundary of the grid must be determined as a function of k_1 and M_∞. In addition, there should be enough grid points per wavelength to accurately represent the airfoil and wake boundary conditions. Due to the harmonic terms which appear in Eqs. (3.57), (3.58), (3.60), and (3.61), it is clear that the η and ξ spacing must also be determined as a function of k_1 and M_∞.

For a given frequency, we use spacing in the η direction which is nearly uniform, with constant spacing on each of the subintervals $0 \le \eta \le 1$, $1 \le \eta \le \eta_{\text{t.e.}-}$, and $\eta_{\text{t.e.}-} \le \eta \le 2$. The spacing on $0 \le \eta \le \eta_{\text{t.e.}-}$ determines the spacing on the airfoil surface. Normally the number of grid points in the η direction varies from 40 for the low frequencies up to about 70 for reduced frequencies of four.

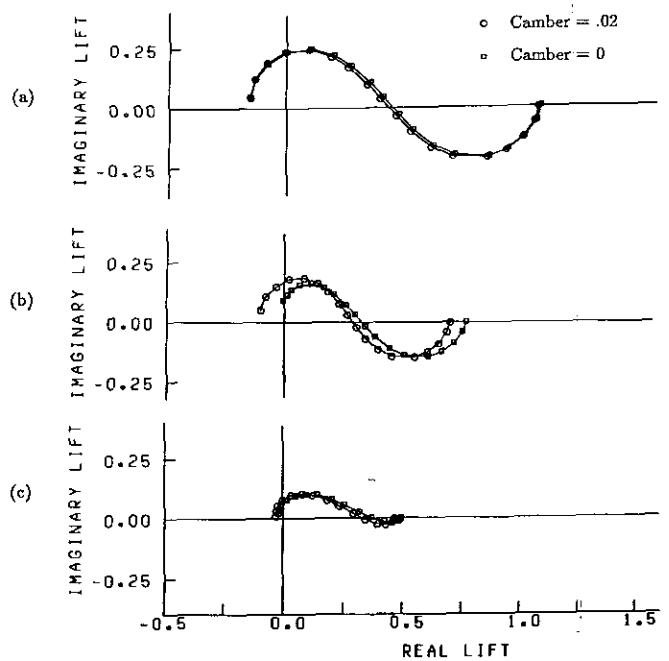

FIG. 19. Comparison between the unsteady lift of an uncambered Joukowski airfoil and an airfoil with camber ratio of 0.02 for (a) a transverse gust, (b) a transverse and longitudinal gust with $-a_1 = a_2 = 0.7071$, $k_1 = k_2$, $a_3 = k_3 = 0$, and (c) a three-dimensional gust with $k_3 = 0.4$, $|\mathbf{a}| = 1$, $a_2/a_1 = -7/4$, $k_1 = k_2$, $\mathbf{a} \cdot \mathbf{k} = 0$, $a_2 > 0$. $M_\infty = 0.1$, $\alpha = 0°$, thickness ratio = 0.12. $k_1 = 0.0, 0.01, 0.03, 0.06, 0.1, 0.2, 0.3, 0.45, 0.6, 0.8, 1.0, 1.3, 1.6, 2.0, 2.5, 3.0, 3.5, 4.0$.

An optimal spacing of the grid points in the wake (the ξ direction) turns out to be more difficult to achieve than the spacing on the airfoil. Numerical studies of the thin airfoil gust response problem showed that the optimal choice of spacing was 12 uniformly spaced grid points per wavelength. For the case of the thin airfoil, the wake boundary condition analogous to condition (3.57) is much simpler, and it is possible to choose the spacing of the ξ grid points such that they are uniformly spaced per wavelength. However, for the general problem of nonuniform mean flows, the waves in the wake are distorted due to the $e^{ik_1} \int_{\Phi_{t.e.}}^{\Phi} (d\Phi/U_0^2)$ term, and it is no longer possible to determine the mesh spacing such that the grid points are uniformly spaced along the waves. This does not prove to be a difficulty, however, because in the far field the general problem of vortical flows past a lifting airfoil reduces essentially to a linear problem as the mean flow tends to become uniform. Thus, we may determine the wake spacing as in the case of the flat plate airfoil, and the grid points will be nearly uniformly spaced per wavelength.

For a flat plate airfoil, the wake boundary condition which imposes continuity of the pressure is given, corresponding to the transformation (3.50), by [15],

$$\psi_{\text{wake},j} = \psi_{\text{t.e.}} e^{i(k_1/\beta_\infty^2)[a^* \cosh(\pi\xi_j) - a^*]}. \tag{3.68}$$

To have uniformly spaced grid points per wavelength, the argument of the exponential function should vary by equal fractional increments of π. To place 12 grid points per wavelength, we are then led to the requirement that the location of the jth ξ grid point be determined from the equation

$$\frac{k_1}{\beta_\infty^2}[a^* \cosh(\pi\xi_j) - a^*] = j\frac{2\pi}{12}. \tag{3.69}$$

Solving for ξ_j, we get

$$\xi_j = \frac{1}{\pi} \cosh^{-1}\left(j\frac{\pi\beta_\infty^2}{6a^*k_1} + 1\right). \tag{3.70}$$

Near the airfoil the above procedure leads to a spacing which is too coarse to be used. In this region we use uniform ξ spacing which remains constant at some value $\Delta\xi$, until a point is reached such that the ξ_j determined from (3.70) satisfy $\xi_{j+1} - \xi_j \leq \Delta\xi$. From that point on, the spacing of the ξ grid points is determined from (3.70)

4. CODE VALIDATION

Extensive efforts were taken to validate the computer codes which were developed to implement the numerical scheme outlined in the previous section. The validation process consisted of a combination of comparing numerical results with known analytical solutions to the classical thin airfoil gust response problem, comparing with the second-order theory of Goldstein and Atassi [4] and Atassi [5], comparing with the first-order numerical results of Atassi and Grzedzinski [18], and calculating solutions to limiting case problems, i.e., as Mach number, thickness, angle of attack, or camber goes to zero.

Sample computation times varied considerably, depending on the reduced frequency, Mach number, and airfoil loading. For thin, unloaded airfoils, with low reduced frequency gusts, typical solution times were about 2 s per frequency on an IBM RS 6000 320 workstation. The higher frequencies for these airfoils required on the order of 5 CPU seconds per frequency, with slightly higher solution times as the Mach number increases. For thick, symmetric, unloaded airfoils, the solution times ranged from about 4 s for the lower frequencies up to about 15 s for the highest frequencies. Finally, for loaded airfoils, the solution times ranged from about 25 s for the low frequencies up to around 120 s for the highest reduced frequencies. No effort was made to optimize the computational efficiency of the scheme, as our main purpose was to validate its accuracy.

In the results that follow, comparisons are made for one-dimensional (transverse) gusts, two-dimensional (transverse and longitudinal) gusts, and fully three-dimensional gusts (see Figs. 6, 7, and 8).

The first step in the validation process was to compare numerical results with classical solutions to the thin airfoil gust re-

sponse problem. In Figs. 9 and 10 we present comparisons between numerical and analytical results for the unsteady lift. The normalized unsteady lift, commonly called the response function, is defined by

$$R_L(k_1, k_2, k_3, M_\infty) = \frac{L'}{\pi \rho_\infty c U_\infty |\mathbf{a}| e^{i\omega t}}, \tag{4.1}$$

where L' is the unsteady lift. Figure 9a shows a comparison between numerical results and the Sears solution [19] for the case of a one-dimensional (transverse) gust in incompressible flow, and Figs. 9.b and 9.c compare numerical results and analytical results obtained from a Possio solver for a one-dimensional gust at Mach numbers of 0.5 and 0.8. The reduced frequency values at which the comparisons are made range from 0 to 4.0 and are shown below the plot. The point on the real axis and furthest to the right corresponds to $k_1 = 0$, and the other points along the curve correspond in order to the other reduced frequency values. Figures 10.a through 10.c compare numerical results and analytical results from a Possio solver for three-dimensional gusts for Mach numbers of 0.1, 0.5, and 0.8. The conditions on the gust wave number parameters are shown below the plots. As can be readily seen, there is excellent agreement between the numerical and analytical results. The only loss of accuracy occurs when both the Mach number and reduced frequency become large. (The apparent loss of accuracy in the incompressible case ($M_\infty = 0.1$) is due to the nonzero Mach number. If $M_\infty = 0.001$, for example, there is virtually no difference between the numerical results and the Sears solution [17].)

To assess the accuracy of the present scheme for nonuniform flows around thin airfoils, we compare with the second-order theory of Goldstein and Atassi [4] and Atassi [5]. The results given by Atassi assume a zero thickness airfoil, but account for the effects of airfoil camber and angle of attack on the airfoil unsteady response. In Fig. 11 we compare the numerically computed response function with the second-order theory for an incompressible flow with a two-dimensional gust about an airfoil with an angle of attack of 2° and a camber ratio of 0.05. The numerically computed response function is for a 6% thick Joukowski airfoil, while the second-order theory does not take into account the airfoil thickness. As can be seen, the numerical results for the 6% thick airfoil show a slightly larger lift at the low frequencies, but a slightly smaller lift at the higher frequencies for k_1 up to about three. As shown in [6, 7], this effect can be attributed entirely to the thickness of the airfoil, so that the agreement is very good for reduced frequencies ranging from zero to three. For frequencies higher than three, it is not possible to make any firm conclusion on the accuracy of the numerical results.

To validate the numerical scheme for airfoils with thickness,

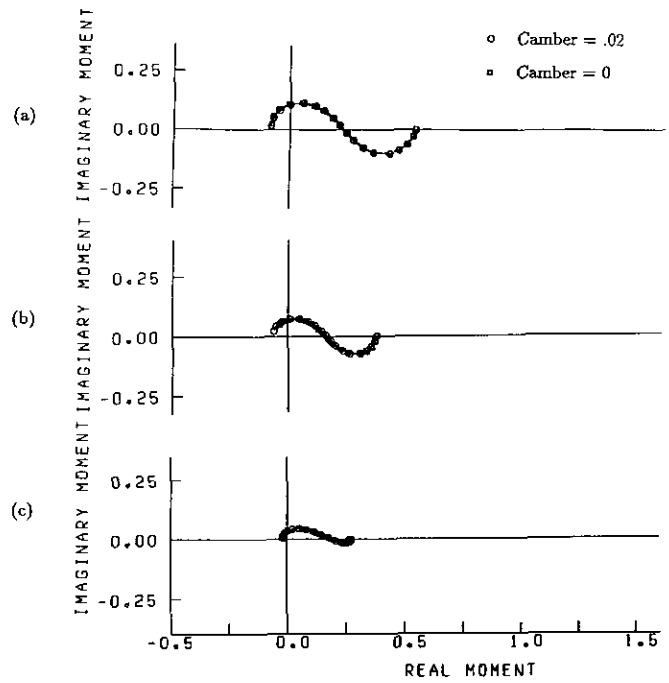

FIG. 20. Comparison between the unsteady moment of an uncambered Joukowski airfoil and an airfoil with camber ratio of 0.02 for (a) a transverse gust, (b) a transverse and longitudinal gust with $-a_1 = a_2 = 0.7071$, $k_1 = k_2$, $a_3 = k_3 = 0$, and (c) a three-dimensional gust with $k_3 = 0.4$, $|\mathbf{a}| = 1$, $a_2/a_1 = -7/4$, $k_1 = k_2$, $\mathbf{a} \cdot \mathbf{k} = 0$, $a_2 > 0$. $M_\infty = 0.1$, $\alpha = 0°$, thickness ratio = 0.12. $k_1 = 0.0, 0.01, 0.03, 0.06, 0.1, 0.2, 0.3, 0.45, 0.6, 0.8, 1.0, 1.3, 1.6, 2.0, 2.5, 3.0, 3.5, 4.0$.

we compare with the results of Atassi and Grzedzinski [18]. In Fig. 12 we show comparisons for one-, two-, and three-dimensional gusts for incompressible flows around a 12% thick Joukowski airfoil with zero degrees angle of attack and zero camber ratio. The reduced frequency values for the comparison range from 0.2 to 2.5. We limit the comparison to this range of k_1, since this is roughly the range of validity of the Green's function approach of Atassi and Grzedzinski. The agreement between the two sets of results is good in general.

The final step in the validation process was to calculate the solutions to various limiting case problems. The limiting case of $M_\infty \to 0$, i.e., the incompressible case, was covered above where the numerical results were compared to the Sears solution. We now present results for the limiting cases of airfoil thickness, angle of attack, and camber.

In Figs. 13–16, we compare numerical results for the unsteady lift and moment about the airfoil center of a 3% thick, symmetric Joukowski airfoil with that of a flat plate airfoil with zero thickness. Analogous to the response function R_L for the unsteady lift, we define the response function R_M for the unsteady moment by

$$R_M(k_1, k_2, k_3, M_\infty) = M' \Big/ \frac{\pi}{2} \rho_\infty c^2 U_\infty |\mathbf{a}| e^{i\omega t}, \tag{4.2}$$

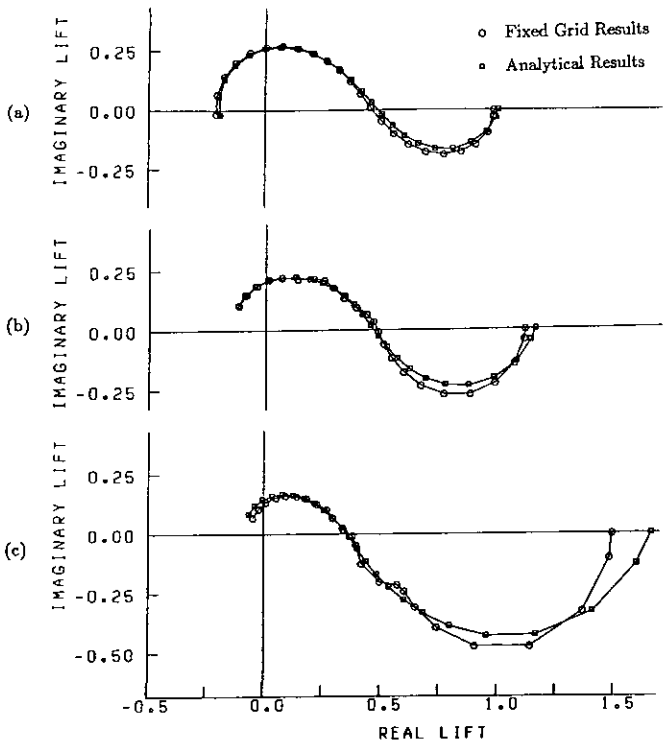

FIG. 21. Comparison between numerical results generated on a fixed grid and analytical results for a flat plate airfoil in a transverse gust at (a) $M = 0.1$, (b) $M = 0.5$, and (c) $M = 0.8$; $k_1 = 0.0, 0.007, 0.027, 0.062, 0.110, 0.172, 0.248, 0.338, 0.442, 0.561, 0.694, 0.842, 1.01, 1.18, 1.38, 1.59, 1.82, 2.07, 2.33, 2.62, 2.93, 3.26, 3.62, 4.01$.

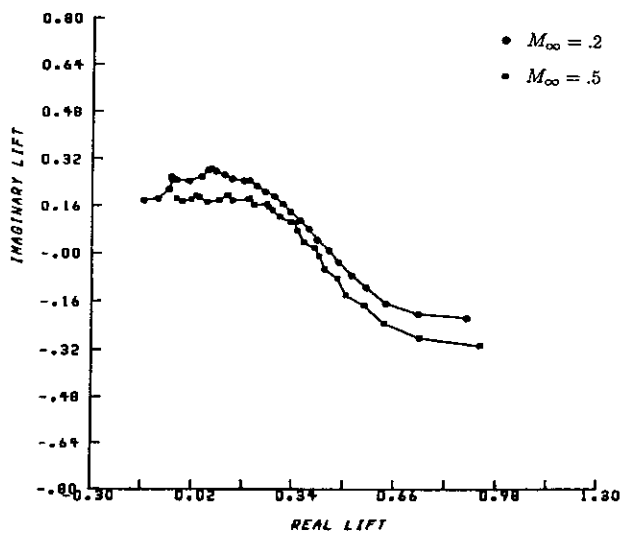

FIG. 22. Numerical results for the unsteady lift of a 12% thick, symmetric Joukowski airfoil in a transverse gust. Results show grid dependent errors due to exponentially decreasing spacing in the ξ direction which was used in place of condition (3.70). $k_1 = 0.1, 0.2, 0.3, 0.4, 0.5, 0.6, 0.7, 0.8, 0.9, 1.0, 1.1, 1.2, 1.3, 1.4, 1.5, 1.6, 1.7, 1.8, 1.9, 2.0, 2.1, 2.2, 2.3, 2.4, 2.5, 2.6, 2.7, 2.8, 2.9, 3.0$.

where M' is the unsteady moment about the airfoil center. Figures 13 and 14 present results for $M_\infty = 0.1$, and Figs. 15 and 16 present results for $M_\infty = 0.6$. For both Mach numbers, it is seen that the small airfoil thickness has little effect on the unsteady response, except for high reduced frequencies in the two-dimensional gust case, where the magnitude of the unsteady lift is reduced by 15–20%. Not surprisingly, thickness effects become more important as the reduced frequency becomes large.

Figures 17 and 18 present comparisons between results for a 12% thick symmetric Joukowski airfoil at zero degrees angle of attack and one degree angle of attack. All plots are for a free stream Mach number of 0.1. As in the case of airfoil thickness, the strongest effect is seen in the two-dimensional gust case. However, here there is a significant effect both for the low and high reduced frequencies. At the low frequency end, the effect is primarily a reduction in the magnitude of the unsteady lift, while at the high end it is primarily a change in phase of the unsteady lift. We also point out that, in agreement with the theoretical results of Atassi [5], for the transverse gust case in which the gust has only an upwash component, the steady loading on the airfoil has virtually no effect on the unsteady lift.

Finally, in Figs. 19–20, we compare results for a 12% thick Joukowski airfoil with no camber with a 12% thick Joukowski airfoil with a camber ratio of 0.02. The free stream Mach number for all plots is 0.1, and the angle of attack is 0°. The effect here is exactly analogous to the effect of small angle of attack, except that it is stronger in this case due to the increased steady loading on the airfoil. For the one-degree angle of attack airfoil the steady lift coefficient was 0.12, while for the 2% cambered airfoil the steady lift coefficient was 0.27. In each case, the reduction of the quasi-steady lift ($k_1 = 0 = k_2$) for the two-dimensional gust is directly proportional to the steady loading on the airfoil with a proportionality constant of 0.26. Using the theoretical results of Atassi reported in [5], it can be shown that for zero thickness airfoils in a two-dimensional gust in incompressible flow, the reduction in the quasi-steady lift for airfoils with small camber and angle of attack is proportional to the steady lift coefficient with a proportionality constant of $(1/\pi)(k_2/|k|) = 0.23$. The difference between the numerical and theoretical values of the proportionality constant can be accounted for by the fact that the theoretical result does not account for the thickness of the airfoil, and, in addition, assumes a parabolic profile for the airfoil camber line.

In Ref. [7], a more general study of how the two-dimensional quasi-steady lift changes in response to mean airfoil loading showed that for heavily loaded airfoils in compressible flow, the value of the proportionality constant was about 0.25. We thus conclude that the reduction in the two-dimensional quasi-steady lift due to mean airfoil loading is roughly proportional to the steady lift coefficient of the loaded airfoil with a proportionality constant of 0.25.

Before concluding, the authors would like to emphasize the

significance of the method of grid determination which was outlined in the previous section. In Fig. 21 we present numerical results which demonstrate the kinds of errors that can occur as a result of using an inappropriate grid. The response functions shown in these figures were generated without determining the grid as a function of the reduced frequency. For each case shown, the same grid was used for all frequencies in the calculation. The grid used for each Mach number was the one normally used only for the highest reduced frequency. By using the grid for the highest frequency, it was assured that there would be sufficient grid resolution to resolve the waves for the lower frequencies. But as can be seen, the agreement is not nearly as good as when the grid is determined as a function of both the Mach number and reduced frequency. These results show the effect of keeping the outer boundary fixed and not varying it with the reduced frequency in order to ensure that the representation of the far-field boundary condition is sufficiently accurate.

The results in Fig. 22 show the kinds of errors that can occur when the grid points are not suitably spaced in the far field. The grids used for the results in Fig. 22 used an exponentially decreasing spacing which was varied to ensure that there were enough grid points per wavelength to adequately model the wavelike structure of the solution. In addition, the location of the far-field boundary was also varied to ensure that the far-field boundary condition would be sufficiently accurate. However, as the results show, there are large errors in the predicted response functions. This is due to the fact that exponential spacing is not suitable for this kind of wave propagation problem.

5. CONCLUSION

In this paper we have presented a finite-difference, frequency-domain numerical scheme for the solution of unsteady, subsonic vortical flows around lifting airfoils. Due to its inherent efficiency and ability to correctly handle the convection and distortion of the upstream vorticity by the nonuniform mean flow, our approach is an ideal solution method for unsteady aerodynamic flow fields.

Among the most important features of our numerical approach are the transformation of the independent variables into elliptic coordinates, the method of determining the unsteady grid as a function of the Mach number and reduced frequency, the far-field radiation condition for the unsteady pressure, and the formulation and method of evaluation of the source term.

The numerical results that we have presented have shown that our scheme can calculate with very high accuracy the solutions to a large variety of unsteady vortical flows. We conclude that for symmetric airfoils and loaded airfoils with small mean loading, the present scheme is very accurate for reduced frequencies ranging from zero up to at least four, for both incompressible and compressible flows. For heavily loaded airfoils, the scheme has similar accuracy for reduced frequencies ranging from zero up to around three. For reduced frequencies above three, it is not possible to make any firm conclusion on the accuracy of our numerical results. This is an area that requires further study.

REFERENCES

1. J. H. Horlock, *Trans. ASME D J. Basic Engng.* **90,** 494 (1968).
2. W. J. McCroskey and P. M.Goorjian, AIAA Paper 83-1691, 1983 (unpublished).
3. W. J. McCroskey, *J. Aircraft* **22,** (3), 236 (1985).
4. M. E. Goldstein and H. M. Atassi, *J. Fluid Mech.* **74,** 741 (1976).
5. H. M. Atassi, *J. Fluid Mech.* **141,** 109 (1984).
6. J. R. Scott and H. M. Atassi, NASA TM 102466, 1990 (unpublished).
7. J. R. Scott, Ph.D. dissertation, University of Notre Dame, April 1990 (unpublished).
8. H. M. Atassi and J. Grzedzinski, *J. Fluid Mech.* **209,** 385 (1989).
9. M. E. Goldstein, *J. Fluid Mech.* **89,** 433 (1978).
10. H. M. Atassi, in *Symposium on Aerodynamics and Aeroacoustics, 1993,* Advanced Series on Fluid Mechanics, edited by K. Y. Fung (World Scientific, Singapore, 1994), p. 121.
11. C. G. Darwin, *Proc. Cambridge Phil. Soc.* **49,** 342 (1953).
12. M. J. Lighthill, *J. Fluid Mech.* **1,** 31 (1956).
13. A. Jameson and D. A. Caughey, in *Proceedings, AIAA 3rd Computational Fluid Dynamics Conference, Williamsburg, Virginia, 1979,* p. 122 (unpublished).
14. H. M. Atassi and J. R. Scott, in *Proceedings, Fourth International Symposium on Unsteady Aerodynamics and Aeroelasticity of Turbomachines and Propellers, Aachen, Germany, 1988,* edited by H. E. Gallus and S. Servaty (Institute für Strahlantriebe und Turbomachine, University of Aachen, Aachen), p. 39.
15. J. R. Scott and H. M. Atassi, NASA TM 101998, 1989 (unpublished).
16. H. M. Atassi, in *Proceedings, Tenth U.S. National Congress of Applied Mechanics, 1986,* edited by J. P. Lamb, (ASME, New York, 1986), p. 475.
17. J. R. Scott and H. M. Atassi, in *Proceedings, Sixth International Symposium on Unsteady Aerodynamics, Aeroacoustics and Aeroelasticity of Turbomachines and Propellers, Notre Dame, Indiana, 1991,* edited by H. M. Atassi, (University of Notre Dame, Notre Dame, Indiana), p. 743.
18. H. M. Atassi and J. Grzedzinski, University of Notre Dame Report, Aerodynamics Group, No. 8, 1986 (unpublished).
19. W. R. Sears, *J. Aero. Sci.* **8**(3), 104 (1941).